Available online at www.sciencedirect.com
SCIENCE DIRECT®
International Journal of Mass Spectrometry 233 (2004) 267–291
International Journal of Mass Spectrometry
www.elsevier.com/locate/ijms

Review

Low energy electron driven reactions in free and bound molecules: from unimolecular processes in the gas phase to complex reactions in a condensed environment

Richard Balog, Judith Langer[1], Sascha Gohlke, Michal Stano[2], Hassan Abdoul-Carime, Eugen Illenberger*

Freie Universitaet Berlin, Institut fuer Chemie—Physikalische und Theoretische Chemie, Takustrasse 3, D-14195 Berlin, Germany

Received 2 October 2003; accepted 23 December 2003

Abstract

Recent results on reactions induced by collisions of low energy electrons (0–15 eV) with molecules at different degrees of aggregation are reviewed. The studies include crossed electron-molecular beam experiments with gas phase molecules under single collision conditions (effusive beams), homogeneous and heterogeneous clusters (supersonic beams), and experiments in the UHV where molecules are adsorbed and condensed in defined quantities on a cryogenic substrate. In single molecules examples of completely selective bond cleavages via dissociative electron attachment (DEA) are presented. Time-of-flight (TOF) measurements of product ions give access to a detailed study of the energy distribution among the fragments. Probing gas phase biomolecules by low energy electrons and its relevance for radiation damage and cancer therapy is discussed. In clusters we present an example of an ion molecule (S_N2) reaction in heterogeneous clusters induced by DEA. In the condensed phase low energy electrons can induce desorption of fragment anions via DEA to molecules at the surface. Examples are given for medium enhanced DEA reactions, controlled modifications of surfaces by low energy electrons and (substrate mediated reactions).

Keywords: Desorption; DEA; Substrate

1. Introduction

Among the various electron initiated processes in molecules, electron capture is a dominating feature at low energies, in particular in the region below electronic excitation [1,2]. At higher energies electron impact can lead to both electronic excitation or ionization. If sufficient excess energy is deposited into the target molecule (neutral or ion) it may decompose into fragments. The total cross section for electron impact excitation or ionization varies smoothly with the electron energy reaching a maximum in the vicinity of 70–100 eV for most molecules [3,4]. The absolute value at maximum can come up to the geometrical cross section of the respective molecule. In contrast to that, the cross section for electron attachment behaves reciprocal with energy [5] and it can hence exceed the geometrical cross section by several orders of magnitude at sufficiently low energies.

Capture of low energy electrons by molecules is an ubiquitous phenomenon in many fields of natural sciences, in the gas phase as well as in the condensed phase or at interfaces. For the gas phase we mention any kind of plasma where electrons in exceeding numbers are present which can drive ionization, excitation and attachment processes [6,7]. In the condensed phase energy deposition by high-energy radiation produces electrons as the most abundant secondary species [8]. The interaction of these *ballistic* secondary electrons with living cells are considered to play a crucial role in the complex reaction sequence leading to genotoxic effects like strand breaks in DNA [9,10]. At the interface solid/vacuum or solid/gas electron initiated processes play a particular role: (i) the photochemistry of adsorbed molecules can strongly be mediated by the transfer of hot electrons from the sur-

* Corresponding author. Tel.: +49-30-838-55350.
E-mail address: iln@chemie.fu-berlin.de (E. Illenberger).
[1] Present address: Institut de Ciència de Materials de Barcelona, E-08193 Bellaterra, Spain.
[2] Permanent address: Department of Plasma Physics, Comenius University, SK-8428, Bratislava, Slovakia.

1387-3806/$ – see front matter © 2004 Published by Elsevier B.V.
doi:10.1016/j.ijms.2003.12.030

face thereby generating a transient negative ion. Adsorbed molecules can hence be photochemically active already at wavelengths below the threshold for gas phase photoabsorption [11]; (ii) tunneling electrons in STM (surface tunneling microscopy) can induce site selective dissociations, or excite selective vibrational modes coupled with surface hopping or desorption [12]. This field, sometimes assigned as *single molecule engineering*, opens many new and interesting prospects with respect to both basic science and application [13].

Capture of a free electron by a molecule generates a *transient negative ion* (TNI) which can be viewed as a molecular quantum state embedded in the electron–target continuum. Such compounds are formed when free electrons of particular energy interact with neutral molecules [1,2]. In the picture of electron scattering theory a resonance is characterized by constructive interferences of the electron wave in the area of the target. In the time dependent description the electron resides in the vicinity of the target for times longer compared to direct (unhindered) propagation across the area of the target. We can thus regard this electron scattering phenomenon as the formation of a short lived negative ion. Since the process is operative at particular energies it is also called *a negative ion resonance* (NIR). Synonymously the term *transient negative ion* (TNI) is used since such a quantum state is principally unstable towards loss of the extra electron (autodetachment). In the approach of molecular orbitals (MOs), the extra electron resides temporarily in one of the normally unoccupied MOs. In competition to loss of the extra electron (autodetachment) a NIR can consequently also dissociate into fragments consisting of one ion and one or more neutrals. The overall process is called *dissociative electron attachment* (DEA), viz.:

$$e^- + M \rightarrow M^{-\#} \rightarrow R + X^- \quad (1)$$

where $M^{-\#}$ assigns the TNI formed via a Franck-Condon transition. If DEA channels are energetically accessible at low energies, the cross section for DEA in the gas phase can reach values exceeding 100 Å^2 (10^{-18} m^2) [5].

In this contribution we shall consider the *formation* of such quantum states, their *energy* and also their *evolution* at different stages of aggregation, namely in single molecules under collision free conditions, in clusters formed by supersonic molecular beam expansion, and on the surface of solids or thin molecular films.

In the gas phase the large cross section for DEA towards low electron energies results from the general energy dependence of the attachment cross section. From very basic principles (Wigner threshold laws [14], scattering of a charged particle from a polarizable target [15]) one expects the capture cross section near threshold to increase with decreasing electron energy ($\sigma \propto \varepsilon^{-0.5}$). These threshold laws, on the other hand, are controlled by the dominant electron–target interaction at larger distances. For neutral gas phase molecules this interaction can be approximated by the charge induced dipole potential:

$$V(r) = -\frac{\alpha e^2}{2r^4} \quad (2)$$

with α the polarizability of the target molecule and r the electron–molecule distance.

The interaction of a low energy electron with a *molecular cluster* can often be described on a molecular site: while at larger distances the electron interacts with the entire cluster, the electron will usually be localized on an individual molecule. For clusters one expects hence (as in single molecules) a reciprocal energy dependence of the attachment cross section near threshold.

For a molecule on a *metallic* surface the situation changes considerably: The metal electrons are redistributed at the surface to screen the field of the external charge due to the approaching electron. The field created by this charge distribution *outside* the metal can be represented by the field of a fictitious charge located *inside* the metal, and having the sign opposite to that of the charge outside the surface (image charge). The associated long-range dipole field is directed perpendicular to the surface and can be expressed as:

$$V(d) = -\frac{e^2}{4d} \quad (3)$$

with d the distance of the electron from the metallic surface.

In a *molecular film* the extra electron will generally become localized on an individual molecule, the interaction can therefore (as in a finite cluster system) be viewed on a molecular site. We have then a negative ion coupled to an environment and the initial resonant state (TNI) can decompose or relax into its ground state. For the attachment cross section near threshold one expects a reciprocal energy dependence, irrespective whether the molecule is located on a metallic surface or at the surface of a molecular film. In the first case (Coulomb interaction (3)) the Wigner law predicts $\sigma \propto \varepsilon^{-1}$ and in the latter case (charge-induced dipole potential (2)) $\sigma \propto \varepsilon^{-0.5}$.

The *energy* of a TNI bound to a cluster or a surface is usually lowered by the attractive polarization interaction of the negative charge with its environment.

Independent of the phase condition the *evolution* of a TNI can principally proceed via the following pathways:

$$M^{-\#} \rightarrow M^{(*)} + e^- \quad (4)$$

$$M^{-\#} \rightarrow M^- + \text{energy} \quad (5)$$

$$M^{-\#} \rightarrow R + X^- \text{ (or } R^- + X) \quad (6)$$

with (4) autodetachment, eventually leaving the neutral molecule in an excited state, (5) relaxation into the stable anion (if existent) and (6) decomposition into stable fragments (DEA). While these processes represent the principle decay channels, it is immediately clear that the branching ratios will be affected by a medium. In the gas phase, for example, relaxation into a stable configuration (process 5), is very unlikely since radiative cooling would be the only

mechanism. Any optical transition in this energy range, however, is by orders of magnitude slower compared to the competing channels (4) and (6). As we shall demonstrate, on the other hand, the competition between autodetachment and dissociation can strongly change on going from the gas phase to a NIR coupled to an environment. In spite of the possibility of efficient energy dissipation within a medium, the lifetime effect can increase the reactivity, i.e., increase the cross section for bond cleavage via dissociative electron attachment for a molecule at a surface (Chapter III.C.2).

The high cross section and selectivity of the DEA reaction (6) can be used to study ion molecule reactions in clusters, for example, binary nucleophilic displacement (S_N2) reactions in a *finite* system bridging the gas phase and condensed phase (Chapter III.B). The rate constant for such reactions can differ enormously between gas phase and solution, in particular cases up to 15 (!) orders of magnitude [16]. This is due to the completely different energy profiles along the reaction coordinate under the different phase conditions.

2. Experimental

The general arrangement to study electron capture reactions with gas phase targets (single molecules and clusters) is schematically shown in Fig. 1. A monochromatized electron beam interacts with the target and ions arising from this interaction are detected mass spectrometrically as a function of the incident electron energy. Information on the distribution of excess energy is obtained by a time-of-flight (TOF) analysis of ionic products (Fig. 2).

Electron stimulated desorption (ESD) of anions is studied in a UHV experiment schematically shown in Fig. 3. Here the target is represented by molecules adsorbed or condensed on a cryogenic surface.

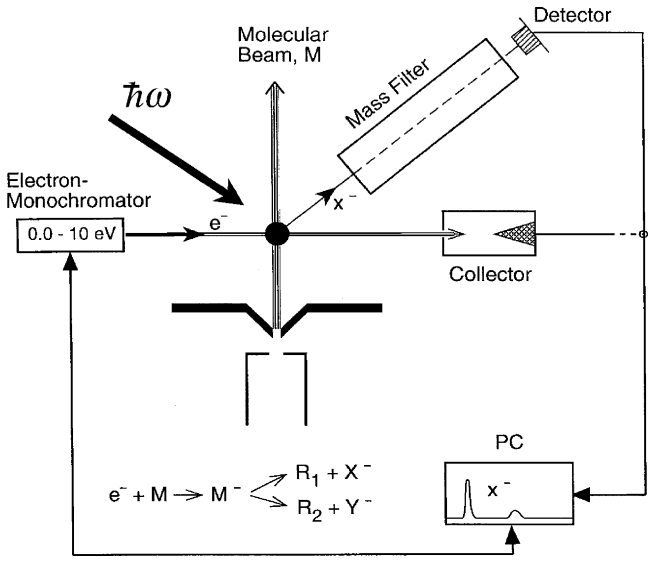

Fig. 1. Schematic arrangement for the study of electron induced reactions in single molecules (effusive molecular beam) or clusters (supersonic beam expansion).

2.1. Isolated molecules and clusters

The gas phase experiments are performed in a crossed electron beam/molecular beam arrangement as described in detail previously [17,18]. The electron beam is generated by a *trochoidal electron monochromator* (TEM) [19] operating with a homogeneous magnetic field which guides the electrons and prevents spreading of the beam which is an essential problem at low energies. The target molecules can be excited by absorption of laser light (IR or UV) to study capture reactions at vibrationally or electronically excited species. Negative ions formed by crossing the electron beam with a molecular beam are extracted from the reaction chamber by a small electric field ($<1\,V\,cm^{-1}$), analyzed by a commercial quadrupole mass spectrometer and detected by single pulse counting electronics. The resolution of the electron beam is in the range 0.1–0.2 eV (FWHM) at a current of ≈20 nA. The electron energy scale is calibrated by means of the 0 eV resonance in SF_6. The molecular beam is either an effusive beam containing single molecules or a supersonic beam formed by adiabatic expansion. The supersonic beam contains a distribution of neutral clusters. The average size can be controlled to some degree by the stagnation pressure and the temperature of the nozzle.

2.1.1. Translational energy release

Information on the translational energy release in gas phase DEA is obtained by a TOF analysis of the ions traveling from the source through the quadrupole mass analyzer to the detector [20]. In brief, the electron beam is now pulsed (pulse width ≈1 μs) and the flight time of the ions (generated within the short time of the electron pulse) from the reaction volume through the quadrupole to the detector is measured. The TOF arrangement, in principle, corresponds to a two-field TOF spectrometer (Wiley-McLaren design [21]) consisting of a draw-out region (draw out field ε_1), an acceleration region (accelerating field ε_2), and the quadrupole mass filter which acts as the drift tube (field free along the flight tube axis $\varepsilon = 0$, Fig. 2).

Ions formed with low kinetic energy (e.g., thermal ions) exhibit one peak in the TOF spectrum while ions generated with considerable kinetic energy produce two peaks due to *direct* and *turn around* ions. In the latter case discrimination

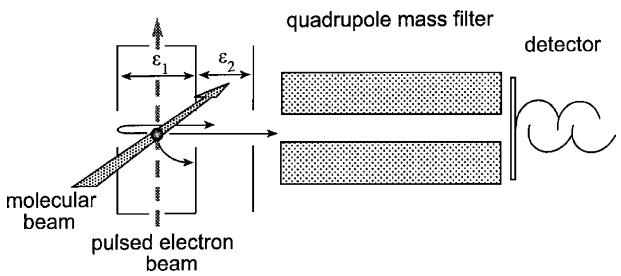

Fig. 2. Schematic of the experimental setup to record TOF spectra of fragment ions. The configuration corresponds to a two field TOF arrangement with the quadrupole acting as a drift tube ($\varepsilon = 0$).

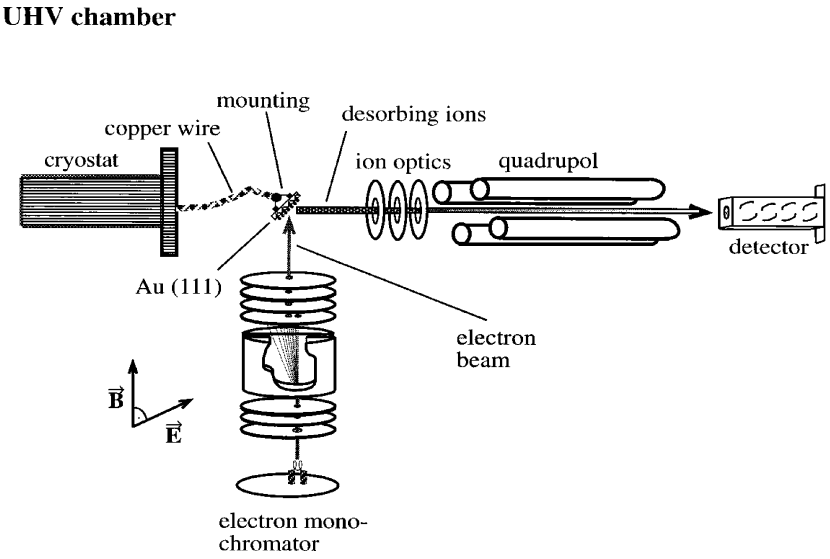

Fig. 3. Schematic of the experimental setup for the study of ESD from adsorbed and condensed molecules. The components are housed in a UHV chamber at a base pressure of 10^{-10} mbar.

against velocity components perpendicular to the flight tube axis results in a separation (in time) of ions ejected parallel (direct) or anti-parallel (turn around) to the axis. The turn around ions are decelerated, reversed, and then accelerated. They hence reach the detector by some time delay (ΔT) with respect to the direct ions. From the experimentally determined flight time difference (ΔT), the initial kinetic energy release of the product ion can be calculated as:

$$E_{\mathrm{T}}^{\mathrm{i}} = \frac{(\Delta T q \varepsilon_1)^2}{8 m_{\mathrm{i}}} \tag{7}$$

where ε_1 is the draw-out field introduced above, q is the elementary charge, and m_{i} the mass of the ion. For a decomposition into *two* particles one can calculate the total translational energy E_{T}, by taking into account the principle of linear momentum conservation leading to:

$$E_{\mathrm{T}} = E_{\mathrm{T}}^{\mathrm{i}} \frac{M}{m} \tag{8}$$

where M is the mass of the parent molecule and m is the mass of the neutral fragment.

Conversely, for ions with sufficiently low kinetic energy there is no discrimination against perpendicular velocity components and all ions are transmitted yielding one single peak in the TOF spectrum.

TOF spectra are recorded by the use of a time-to-pulse height converter (TPHC) followed by analog/digital (ADC) conversion.

2.2. Adsorbed and condensed molecules

The electron stimulated desorption experiments are carried out in a UHV apparatus with a base pressure in the chamber in the 10^{-10} mbar range. The arrangement consisting also of a TEM, a cryogenic cooled monocrystalline Au substrate mounted on a manipulator and a commercial quadrupole mass spectrometer with an ion extraction system (Fig. 3). The substrate can be cooled down to approximately 40 K (measured by a thermocouple directly mounted at the crystal) by means of a closed cycle He refrigerator and resistively heated up to several hundred Kelvin. The molecules are condensed on the metallic substrate by exposing it to a volumetrically calibrated gas quantity effusing from a capillary located 0.7 cm from the crystal. Molecules can be deposited either directly on the metallic substrate or on a multilayer rare gas film as a spacer to the metal.

The electron energy is calibrated by the onset of electron transmission into the metallic substrate (0 eV, vacuum level). From the steepness of the onset curve the energy width of the electron beam can be estimated as 0.2 eV at a current of ≈50 nA. Exposure of a molecular film to the electron beam can lead to accumulation of negative charges due to stabilized parent anions, fragment anions and otherwise trapped electrons. This results in a shift of the electron injection curve with respect to the monochromator potential. All desorption spectra shown are calibrated with respect to the onset of the injection curve. Charge accumulation, however, is always associated with some broadening of the injection curve [22], most likely due to inhomogeneous charging of the sample area.

3. Results and discussion

3.1. Single molecules under collision free conditions

3.1.1. Selective bond cleavage in CF_3I and C_2F_5I

The two perfluoroiodo compounds show strong DEA signals on the I^- channel near 0 eV (Figs. 4 and 5) with absolute cross sections of approximately 3×10^{-14} cm^2 in CF_3I

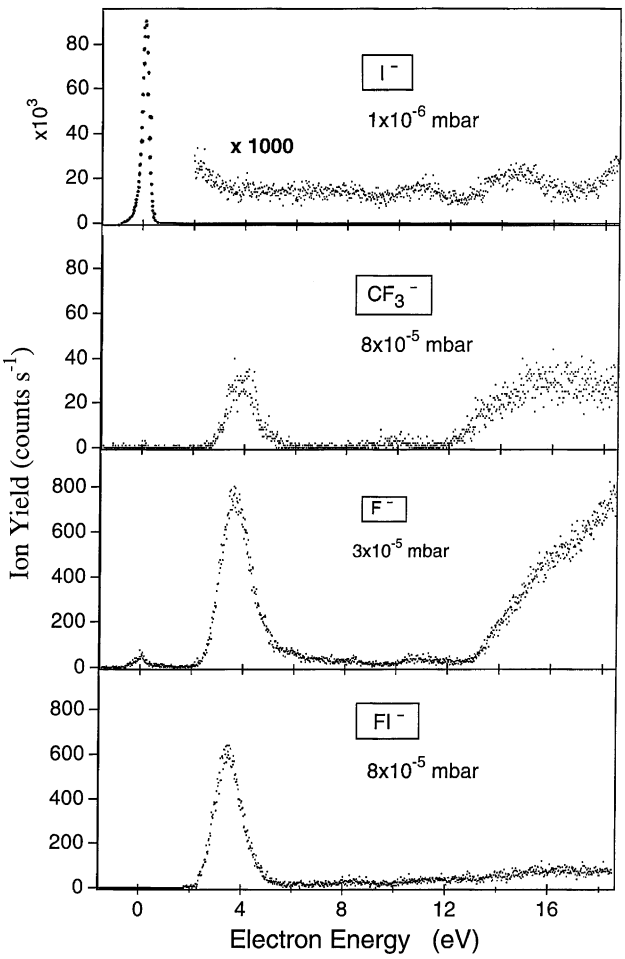

Fig. 4. Ion yield curves from electron attachment to single CF_3I molecules. Note that the I^- spectrum was recorded at a reduced gas pressure. The normalized intensity ratio I^-: CF_3^- is thus $\approx 2 \times 10^5$. The small F^- peak near 0 eV is probably due to thermal decomposition of the molecule at the hot filament generating F_2 which then undergoes DEA (adapted from Ref. [23]).

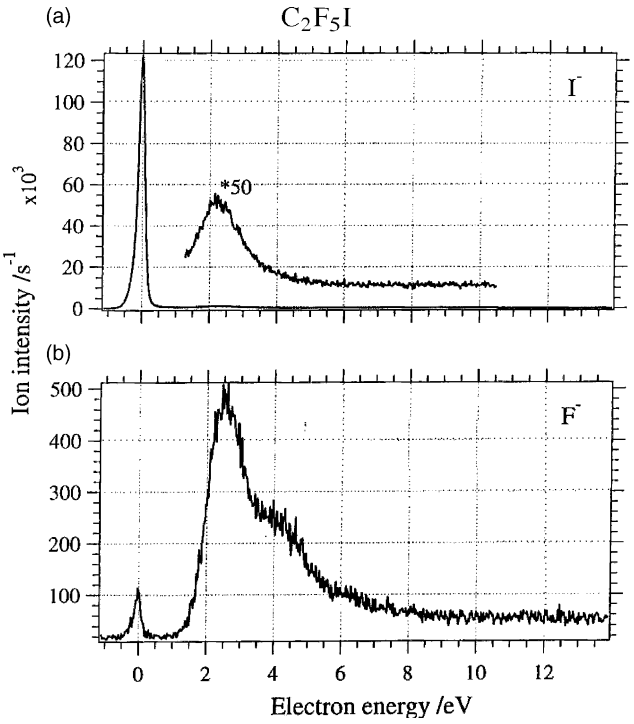

Fig. 5. Ion yield curves from electron attachment to single C_2F_5I molecules (adapted from Ref. [25]).

[23] and 2×10^{-15} cm^2 in C_2F_5I [24,25]. It must be emphasized that in the present molecules the cleavage of the C–I bond near 0 eV is completely *selective* since other DEA channels are energetically inaccessible. In addition the cross section for the reaction in both molecules is considerably larger than their respective geometrical cross section.

One of the chemist's ultimate goals has always been to prepare a system in a specific way to induce a particular reaction which is often initiated by a particular bond cleavage. Many methods and tools have been used within the last decades in that direction. We mention here mode selective vibrational excitation by IR lasers, site selective inner shell excitation by synchrotron radiation or controlled electronic excitation by laser irradiation. A very timely approach to control a photo initiated reaction is the application of ultrashort laser pulses. The idea here is to find the optimum pulse shape (and hence the optimum phase correlation between the frequencies) to push a reaction into the desired direction. By the use of an evolutionary algorithm to create the optimum pulse shape it has in fact been demonstrated that in organometallics different bond cleaving reactions can be selected [26]. Such studies are currently extended from the gas phase to solution [27].

On the other hand, the present molecules dissociate at 100% selectivity following electron capture according to:

$$e^-\,(0\,\text{eV}) + CF_3I \rightarrow CF_3I^{-\#} \rightarrow I^- + CF_3 \quad (9)$$

$$e^-\,(0\,\text{eV}) + C_2F_5I \rightarrow C_2F_5I^{-\#} \rightarrow I^- + C_2F_5 \quad (10)$$

since further competing channels become open only at appreciably higher energy (e.g., $CF_2I + F^-$ above $\approx$1.5 eV). While such a situation can in principle also be established in any neutral or positively charged molecule, the particular situation here is that the reaction is *selective* but also very *effective*. While the selectivity of the reaction is simply due to energetics, its effectivity stems from the general reciprocal energy dependence of the attachment cross section (see above). In contrast to that, excitation or ionization cross sections increase gradually above the corresponding energy threshold. Figs. 5 and 6 both indicate some weak F^- signal at $\approx$0 eV which is *not* due to primary DEA at the target molecule. At this point, we shall not discuss the delicate problem of weak 0 eV peaks in any detail. In the present case this signal may arise from thermal decomposition producing F_2 which can undergo effective low energy DEA for those F_2 molecules reaching the reaction chamber.

In terms of the MO picture, low energy electron capture proceeds via strongly localized σ^*(C–I) antibonding MOs. Such transient anions undergo *impulsive* unimolecular frag-

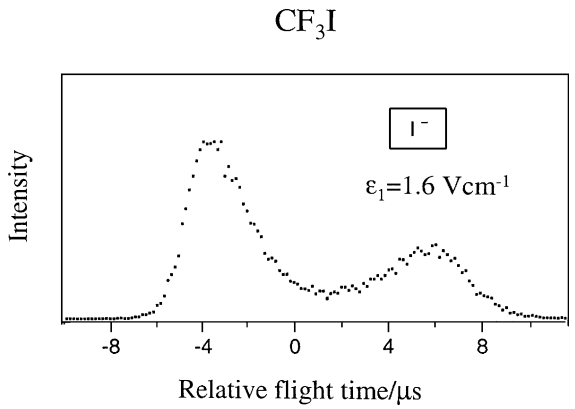

Fig. 6. TOF spectra of I^- from CF_3I recorded at an electron energy of ≈0 eV. Flight time 0 refers to an I^- ion without initial translational energy ($E_T^i = 0$). The well separated doublet is reminiscent of a *quasi discrete* translational energy distribution.

mentation into I^- and the corresponding radical (see the description later).

Both compounds possess resonances at higher energies associated with further fragmentation pattern [23,24] which we shall not discuss here. These resonances are associated with electronically excited negative ion states (core excited resonances).

3.1.1.1. Energy balance in dissociative electron attachment to CF_3I and C_2F_5I. Knowledge of the distribution of the available excess energy among the different degrees of freedom in the fragments (internal and translational energy) provides insight into the mechanism and dynamics of the unimolecular decomposition process [28,29]. The necessary prerequisite to obtain information on the energy distribution is knowledge of the total energy deposited into the precursor molecule. The unimolecular decomposition of *ions* (in particular in photoionization) has been studied since several decades [29–38] as ions are easy to handle and to detect. In photoionization of a polyatomic molecule (M), for example, the parent cation $M^{+(*)}$ may decompose into fragments.

$$\hbar\omega + M \rightarrow M^{+(*)} + e^- \quad (11a)$$

$$\rightarrow R + X^+ \quad (11b)$$

if it contains sufficient energy to access the dissociation limit $R + X^+$. In order to control the energy content in the precursor ion $M^{+(*)}$ for a particular photon energy, coincidence techniques are commonly used [36–38]. At a given photon energy the ion (parent or fragment) is then detected *in coincidence* with the photoelectron of particular energy. Numerous investigations concerning the unimolecular dissociation of cations have been performed with the aim to test theories but also to find means to control such reactions.

It has to be emphasized that in electron attachment the energy of the precursor ion is completely controlled by the energy of the attaching electron. The energy balance in the unimolecular decomposition of transient anions can hence directly be studied. To study the excess energy distribution in DEA in the two perfluoroiodo compounds, we restrict to the selective reactions (9) and (10) at ≈0 eV and analyze the flight times of the I^- ions.

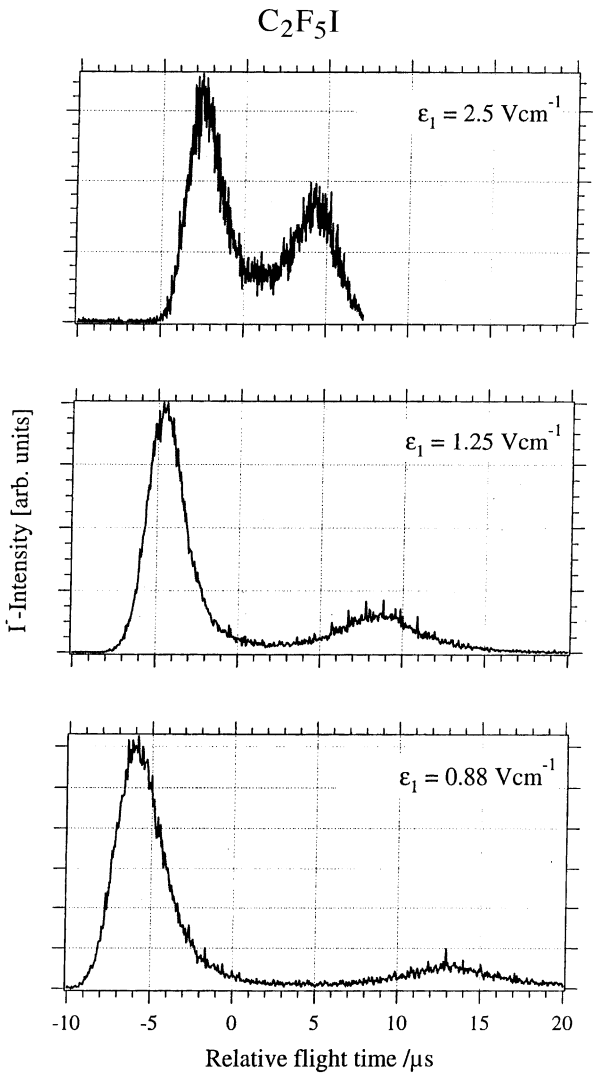

Fig. 7. TOF spectrum of I^- from C_2F_5I recorded at ≈0 eV electron energy and different ion draw out fields (adapted from Ref. [25]).

Fig. 6 shows the TOF distribution of I^- from CF_3I recorded at ≈0 eV and at a draw out field of 1.6 V cm^{-1}. In Fig. 7 TOF spectra of I^- from C_2F_5I are plotted, also recorded at ≈0 eV but at different ion draw out fields. Both systems show separated peaks due to direct and turn around ions. A TOF doublet is reminiscent of both an appreciable kinetic energy release but also the fact that the distribution of translation energy is narrow (*quasi discrete*). At stronger draw out fields, initial velocity components perpendicular to the flight tube axis will successively contribute to the signal thus smearing out the two peaks. In addition, turn around ions become less discriminated as obvious from trajectory calculations [2].

The evaluation of a series of TOF distributions for both systems on the basis of Eq. (7) results in a translational energy for the I^- fragment of $E_T^i = (230 \pm 20)$ meV when ejected from CF_3I and $E_T^i = (250 \pm 20)$ meV from C_2F_5I. Taking into account linear momentum conservations this leads to a total translational energy for both fragments of $E_T = (580 \pm 50)$ meV ($I^- + CF_3$) and $E_T = (520 \pm 45)$ meV ($I^- + C_2F_5$). With the well established thermodynamic data [39] the reaction enthalpy of process (9) is obtained as −670 meV and that of (10) as −790 meV. The total available excess energy at 0 eV electron energy is hence $E^* = 670$ meV and $E^* = 790$ meV for reaction (9) and (10), respectively. From that it follows that (87 ± 6)% of the available excess energy appears as translational energy ($E_T/E^* = 0.87 \pm 0.06$) in the decomposition of CF_3I while in C_2F_5I it is (66 ± 6)%.

It must be noted that on the basis of the statistical treatment of unimolecular reactions one would expect a much lower value. In this approach one assumes that the energy is completely randomized in the precursor complex and that the relative translational energy of the products entirely arises from the kinetic energy located in the reaction coordinate. The simplest solution of the RRKM-QET treatment [29] yields the expression $E_T = E^*/N$ with N the number of normal modes in the precursor complex. Here E_T assigns the *mean* translational energy of a distribution $f(E_T)$ having the most probable energy at zero and falling off continuously towards higher energy.

The appreciable translational energy release and also the appearance of a quasi discrete distribution (with the maximum at some finite value) indicates that the unimolecular process cannot be described within the QET treatment, but rather as direct electronic dissociation along a repulsive potential energy surface. This is also obvious from the involvement of the localized σ*(C–I) MO. In other words, the unimolecular process of the molecular ion is characterized by initial *charge* and *energy* localization at that bond which is cleaved and consequently a statistical description of its decay is not appropriate.

Impulsive dissociation processes can be described in terms of two limiting cases, the *soft radical* limit and the *rigid radical* limit [40,41]. In the first case it is assumed that in the initial step the C atom and I^- ion recoil with the full available energy E^*. In the second step, the carbon atom runs into the rest of the radical exciting the internal degrees of freedom in the neutral radical. This limit predicts the maximum amount of energy to be transferred as internal energy into the molecular fragment in the case of a completely local excitation (impulsive dissociation). The final translational energy is then solely determined by conservation of energy and momentum leading to:

$$\frac{E_T}{E^*} = \frac{\mu(\text{I–C})}{\mu(\text{I–R})} \tag{12}$$

with μ(I–C) the reduced mass between the recoiling particles (first step) and μ(I–R) that between iodine and the corresponding radical (CF_3, C_2F_5). For CF_3I the soft limit predicts that 25% of the available energy emerges as translational energy and for C_2F_5I it is 18%. Note that this value (based on the *impulsive soft radical limit*) is even above that predicted by the statistical treatment.

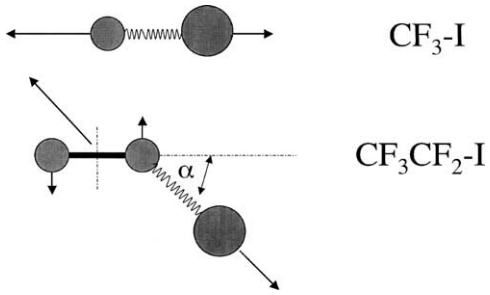

Fig. 8. Decomposition of CF_3I and C_2F_5I along the repulsive C–I coordinate. In C_2F_5I this leads to rotational excitation (see the text).

The experimental observation, on the other hand, indicates that 87% (CF_3I) and 66% (C_2F_5I) of the available energy appears in the translational mode indicating that both systems behave close to the rigid radical limit. This may be understood by the comparatively weak C–I repulsion as opposed to the stronger C–F interaction resulting in a coupling to only soft vibrational modes within the short dissociation time (some tenth of femtoseconds).

From symmetry reasons both systems behave differently with respect to excitation of internal degrees of freedom. While the symmetry of CF_3I (C_{3v}) dictates that internal energy of the fragment CF_3 can only appear as vibrational energy, dissociation of $C_2F_5I^{-\#}$ must be accompanied with rotational excitation of the C_2F_5 radical (see Fig. 8).

By taking into account conservation of energy and (linear and angular) momenta, and treating the neutral radical (C_2F_5) as a rigid rotor, the ratio between rotational energy in the fragment, E_{rot}, and total excess energy, E^*, can be expressed as [40]:

$$\frac{E_{rot}}{E^*} = \frac{1}{1 + (\theta/\mu R^2 \sin^2\alpha)} \tag{13}$$

θ is the moment of inertia of the radical (C_2F_5), μ is the reduced mass between the two fragments (I/C_2F_5), R is the distance between the rotational axis (the center of gravity of the radical) and the C atom connected to the I atom (the lever arm) and α is the angle between R and the C–I axis (Fig. 8). Using the typical bond length d(C–C) = 1.50 Å we obtain $R = 0.87$ Å which is more than half of the C–C distance. Taking d(C–F) = 1.30 Å and assuming an angle C–C–F of 120° for each of the five F atoms we obtain the moment of inertia as $\theta = 205$ amu Å^2 corresponding to a rotational constant of $B = 0.08\,\text{cm}^{-1}$. With $m = 61.4$ amu we arrive at $E_{rot}/E^* = 0.15$, i.e., the approximation predicts that 15% of the total energy is transferred into rotational energy which means that 19% must be stored in vibrational modes.

It is interesting to note that UV photodissociation of both CF_3I and C_2F_5I results in a similar impulsive dissociation [41,42] with most of the available energy as recoil energy

between the radical and the iodine atom, the latter almost exclusively in the excited spin orbit state I^* ($^2P_{1/2}$). The lowest transition (HOMO–LUMO) in the alkyl halides corresponds to excitation of an essentially nonbonding πp orbital on the iodine atom to the antibonding σ*(C–I) MO. The situation is hence comparable to electron attachment with one more electron in the system.

The present results demonstrate that DEA can be 100% selective with respect to the cleavage of a particular bond. Since the total energy of the system is completely controlled by the electron energy, one has direct access to the energy distribution of the unimolecular decomposition. Measuring the translational energy of the fragment ion then allows detailed information of the distribution of the excess energy among the degrees of freedom in the fragments.

3.1.2. Probing gas phase biomolecules by low energy electrons

The interaction of low energy electrons with biomolecules is directly related to the old problem of radiation damage. After the discovery of X-rays, radioactivity and nuclear fission it became soon obvious that the exposure of living beings to high energy radiation (particles and photons) can result in fatal effects for the concerned individual. The variety of such effects is subsumed under the term *radiation damage*. It includes damage of biological material on a short time scale, i.e., the immediate collapse of living cells eventually resulting in the death of the individual within hours or days but also effects appearing on a much longer time scale. Instead of a complete damage of cells, radiation can result in genotoxic effects, i.e., change the genetic expression of DNA or strand breaks.

Countless numbers of articles have been published in relation to radiation damage. Here we only refer to an older [43] and three recent monographs [44–46]. It appears that phenomenological aspects of radiation damage are well documented. There is, however, a very fundamental lack in the description of the initial steps following irradiation. Recently, there is much interest in the interaction of low energy electrons with biomolecules since it was shown that subionization electrons can effectively induce single and double strand breaks in plasmid DNA [10].

3.1.2.1. Primary and secondary processes in living cells. The most important component of the cell nuclei is DNA in which genetic information is stored. To understand the effect of high energy radiation to a living cell (DNA and its environment) one may follow this primary interaction through the secondary reactions in a chronological order. As an example, consider a bunch of photons at energies in the MeV range interacting with DNA and its environment (Fig. 9). The *primary* photon interaction (absorption, scattering) removes electrons from essentially any occupied state, from valence orbitals to core levels. Depending on the energy of these ionized electrons they induce further ionization events, etc. thereby being slowed down. The estimated quantity is

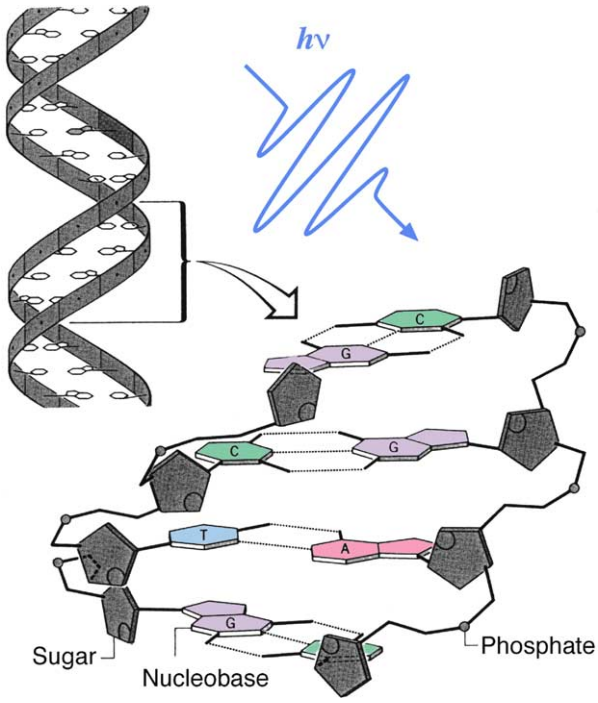

Fig. 9. A pulse of high energy radiation interacting with DNA and its environment (see the text).

10^4 *secondary* electrons per 1 MeV primary quantum [10]. These electrons are usually assigned as *secondary* although they are the result from primary, secondary, tertiary, etc. interactions, including electrons from Auger processes generated during relaxation of the core holes. Taking a snapshot at some femtoseconds after the primary interaction we have then multiple charged sites within the complex molecular network (eventually undergoing Coulomb explosion), single ionized and electronically excited sites and, last but not least, an exceeding number of low energy secondary electrons with an energy distribution extending to a few tenth of eV [10]. Although the double and single ionized sites as well as electronic excitation can result in the rupture of chemical bonds, the major effects are induced by the large number of secondary electrons. In the course of successive inelastic collisions within the medium they are thermalized within picoseconds before they reach some stage of solvation, then as chemically rather inactive species.

Damage of the genome in a living cell by ionizing radiation is about one third *direct* and two third *indirect*. Direct damage concerns reactions by energy deposition directly in the DNA and its closely bound water molecules. Indirect damage results from energy deposition in water and other biomolecules in the surrounding of the DNA. It is believed that almost all the indirect damage is due to the attack of the highly reactive hydroxyl radical OH.

3.1.2.2. Electron initiated reactions in DNA bases. DNA is a biopolymer consisting of two chains (strands) containing the four heterocyclic bases thymine (T), adenine (A), cyto-

sine (C) and guanine (G), each of them bound to the DNA backbone which itself is composed of phosphate and sugar units. Both strands are connected through reciprocal hydrogen bonding between pairs of bases in opposite positions in the two strands. The geometry is such that adenine pairs with thymine (A–T) and guanine with cytosine (G–C) resulting in the well recognized double helix form. The DNA itself is surrounded by other biomolecules (proteins) and water.

In order to reveal the mechanism of DNA damage, the first step would be to investigate the interaction of low energy electrons with single DNA bases representing the building blocks of the large polymer. In an effort to describe these effects on a molecular level, different laboratories started programs to probe building blocks of biomolecules in the gas phase [47–50]. The question then is to which degree these *intrinsic* properties (as revealed by gas phase studies) can be transferred to its analogue in solution. This problem has been a longstanding issue in many areas of *Physical Chemistry*. One has to keep in mind that the solvent represents a dissipative environment, and in reactions where charged particles are involved, solvation can considerably modify the energy profile of the reaction coordinate.

For the study of electron attachment to gas phase molecules two methods have been applied so far (i) crossed electron/molecular beam experiments with mass spectrometric detection of the anions formed [47,49,50] and (ii) electron transmission (ET) through a gaseous sample of biomolecules [48]. While ET mirrors the initial Franck-Condon transition and hence the energy of the precursor ion, the mass spectrometric detection reflects the two step process of DEA, the initial transition forming the TNI and its decomposition into the particular ionic fragment.

In our experiment the molecular beam is generated by moderately heating the powder sample containing the DNA bases to 150–200 °C and effusing the molecules through the collision region. The ions resulting from the electron–molecule collisions are extracted from the interaction region and focused onto the entrance of a mass filter where they are analyzed and detected.

As an example Fig. 10 shows electron attachment to the DNA base thymine (T) leading to the most dominant fragment $(T–M)^-$ formed by abstraction of a neutral hydrogen atom with the negative charge remaining on the ring, viz.:

$$e^- (\approx 2\,eV) + T \rightarrow T^{\#-} \rightarrow (T–H)^- + H \quad (14)$$

with a resonance maximum near 1 eV and a threshold close to 0.5 eV. The absolute cross section for this DEA cross section can be estimated as $\sigma_{DEA} \approx 4\,Å^2$ ($4 \times 10^{-20}\,m^2$) which is in the same order of magnitude as the geometrical cross section of the molecule.

Effective dehydrogenation is a general feature in low energy electron induced reactions to DNA bases and also other biologically relevant molecules like amino acids [51]. The reaction is driven by the large electron affinity of the corresponding radical (M–H) which in the case of the DNA bases is in the range of 3.0–3.5 eV [52]. Electron impact to

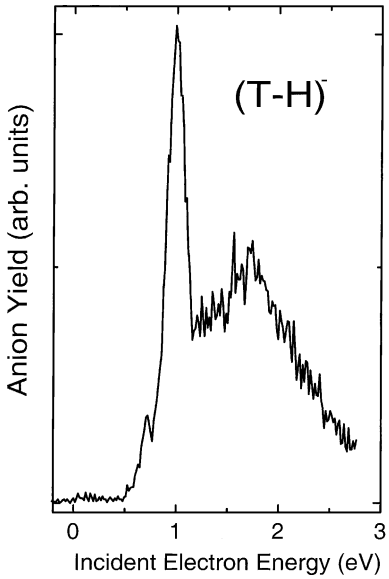

Fig. 10. Dissociative electron attachment to thymine (T) leading to the dominant channel of dehydrogenation with ejection of a neutral hydrogen radical and the charge remaining on the ring creating the closed shell thymine anion $(T–H)^-$.

DNA bases at higher energy results in DEA fragmentations involving opening of the cycle unit [52]. While from these experiments the route to genotoxic effects like strand breaks is not directly obvious and may involve a sequence of reactions, the present experiments clearly show the propensity of electrons (i) to induce fragmentation and produce reactive radicals at subexcitation energies (<3 eV) and (ii) to induce ring opening reactions at subionization energies (<10 eV).

3.1.2.3. Radiation damage and radiosensitizers for tumor therapy. While high energy radiation can damage biological material, radiation is, on the other hand, successfully used in tumor therapy. The problem here is to only expose the affected material but keep the other areas non-irradiated. One way of potential treatment is the use of *radiosensitizers* with the effect that the sensitized cells will collapse already at dosages leaving the healthy material essentially unaffected. The necessary prerequisite for effective therapy strategies, however, is the understanding of the molecular mechanisms of the underlying processes. We shall illustrate this issue for the case of radiation damage which is in turn directly associated to the question of the molecular mechanism by which a radiosensitizer operates.

We shall consider here a prototype gas phase result to illustrate the effect when the DNA base thymine (T) is replaced by bromouracil (BrU). It has been known for many years that substitution of T by BrU in the genetic sequence of cellular DNA (Fig. 11) leads to a greater sensitivity to ionizing radiation without changing the gene expression in non-irradiated cells. Hence bromouracil possesses potential application as a tumor specific sensitizer in cancer therapy. On proceeding from higher energies to low energies the fol-

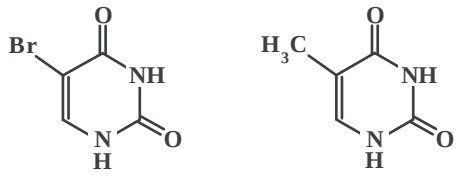

Fig. 11. In bromouracil (BrU) the methyl group in thymine (T) is replaced by Br.

lowing features in electron impact to T and BrU become apparent:

(I) The ionization and excitation cross sections for both compounds behave *usual*, i.e., they rise gradually above the corresponding threshold with total values remaining below the geometrical cross section of the molecule. Ionization and electronic excitation can also result in fragmentation but this area is still fairly unexplored.
(II) While T and BrU behave quite similar at energies above electronic excitation, there are remarkable differences in the subexcitation region. The common feature is that both molecules exhibit pronounced resonance features due to resonant electron attachment but at much different cross sections.

In thymine (T) the most abundant channel was identified as dehydrogenation (reaction (14)). In contrast to that, the radiosensitizer bromouracil exhibits a very intense and narrow low energy resonances (Fig. 12) located close to 0 eV [53] and associated with the processes:

$$e^-\,(0\,eV) + BrU \rightarrow BrU^{\#-} \rightarrow (U\text{-yl}) + Br^- \quad (15a)$$

$$e^-\,(0\,eV) + BrU \rightarrow BrU^{\#-} \rightarrow (U\text{-yl})^- + Br \quad (15b)$$

which are complementary with respect to the negative charge. (U-yl) denotes the fragment formed by the loss of bromine. (15a) is the most abundant channel with an estimated cross section of 600 Å^2 (6×10^{-18} m^2). Reaction (15b) is also operative at 0 eV (though at only 6% of the intensity of (15a)). Due to the appreciable electron affinities of Br and (U–yl) exceeding 3 eV, these reactions have low energy thresholds. Fig. 12 also shows that the undissociated anion weakly appears within the time scale of the experiment (ca. 50 μs).

It is interesting to note that both T and BrU are damaged at electron energies below 3 eV. The absolute cross sections, however, differ by more than two orders of magnitude. The conclusion then is that the initial mechanism for *direct* DNA damage is bond cleavage by low energy secondary electrons which is much more effective in the radiosensitizers.

3.1.2.4. Gas phase results and biological reality. The general question remains to which degree such gas phase results are relevant for a real (in vivo) biological system. DNA as a polymer is embedded in a medium while the present reactions are observed from isolated gas phase components. In the following we consider a few points.

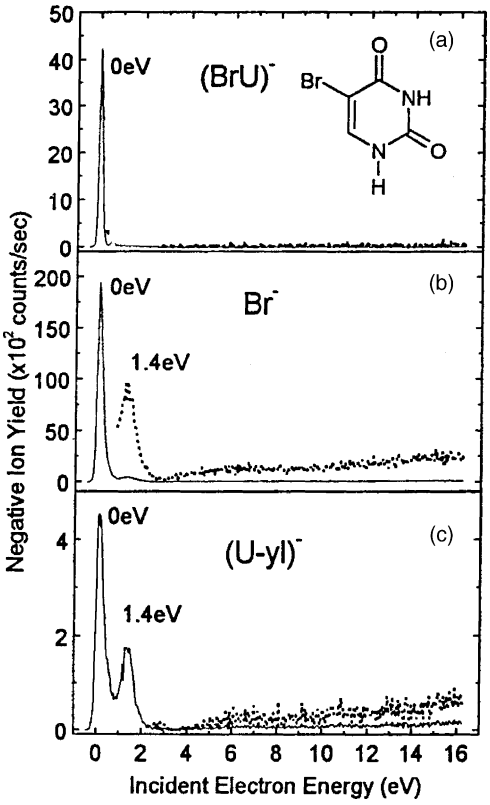

Fig. 12. Electron attachment to the radiosensitizer BrU. In addition to the complementary DEA channels an undissociated parent anion BrU$^-$ is observed at low energy (adapted from Ref. [53]).

(I) Coupling of the nucleobases to the backbone and the opposite chain will certainly modify the energy of the involved molecular orbitals to some degree but one can assume the essential DEA features of the isolated bases will remain in the polymer.
(II) In a condensed environment the reactivity (bond cleavage) is usually suppressed due to energy dissipation, but there are also situations where bond rupture via low energy attachment can be enhanced by the medium (Chapter III.C.2). Irrespective of the phase condition, however, one can assume that BrU remains the more effective dissociative electron scavenger with respect to T which explains the mechanism by which BrU operates as radio sensitizer [54].
(III) The reaction route from dissociative electron capture to single and double strand breaks is not directly obvious and has to be explored. This can be done by studying electron interactions with DNA model systems like small oligonucleotides with defined composition and sequence [55].

We finally mention that electrons in the solvated stage can be viewed as chemically rather unreactive species. The binding energy of those electrons in water is above 3 eV

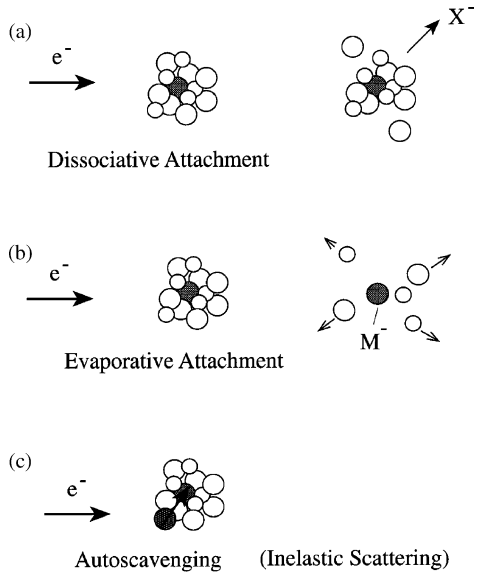

Fig. 13. Illustration of some electron induced processes in clusters (see the text).

and hence any dissociative electron transfer associated with reactions of the form (15a) and (15b) are associated with a large activation barrier and may not play any significant role.

On a superficial view it seems paradoxical that the damage of high energy radiation in the million eV range is actually the result of the interaction of secondary electrons at very low energies. Capture of electrons into antibonding molecular orbitals, however, is a very effective means to transfer energy of the light electron into motion of the heavy nuclei.

3.2. Van der Waals clusters

The interaction of electrons with aggregated molecules is principally a multiple-scattering problem since in the energy range relevant here, the *de Broglie* wavelength of the incoming electron is larger or comparable to the intermolecular distances (the *de Broglie* wavelength of a 1 eV electron is 12.4 Å), the electron wave is simultaneously scattered at different targets.

Although principally a multiple-scattering problem, the cross section for the formation of a negative ion from clusters usually exhibit *resonances* which can be described on a molecular site, i.e., formation and decay of an individual TNI, coupled to the environmental molecules [56]. In spite of that the situation with respect to isolated molecules becomes appreciably more complex and Fig. 13 illustrates some out of a variety of possibilities.

(I) Electron capture generates an individual TNI within the target cluster decomposing into a neutral and negatively charged fragment. If formed with sufficient kinetic energy, the fragment ion may leave the cluster and will be detected. Its translational energy is usually lowered [56] due to collisions which also results in evaporation of monomer units.

(II) Alternatively intra cluster collisions can stabilize the TNI into its relaxed (thermodynamically stable) configuration. This leads to the observation of parent anions which cannot be generated in electron attachment to single molecules under collision free conditions. The transfer of relaxation energy within the cluster results in the evaporation of monomer units (evaporative attachment).

(III) At higher electron energies the incoming electron can first be scattered at one component of the cluster before localization. In the case of inelastic scattering, excited states or resonances coupled with the excitation of the neutral molecule become visible on the final ionic product.

Further possibilities which are not shown in Fig. 13 include:

(IV) Ion–molecule reactions in the cluster where a particular ion can be generated by DEA. A prototype reaction is the so called bimolecular nucleophilic displacement (S_N2) reaction which can be initiated by DEA in a van der Waals cluster (see the description later).

(V) Formation of *solvated electrons* if the cluster consists of molecules with sufficient polarity. Such experiments have been performed in clusters of H_2O and NH_3 [57–61].

In this chapter we restrict to the study of an (S_N2) reaction as example from (IV) which also includes relaxation phenomena.

3.2.1. Intra cluster ion–molecule reactions

The classical bimolecular nucleophilic displacement (S_N2) reactions of the form:

$$X^- + RY \rightarrow [XRY]^{-\#} \rightarrow XR + Y^- \quad (16)$$

can readily be studied in a crossed electron/molecular beam experiment with the molecular beam containing mixed neutral clusters of the components A and B [62]. The nucleophile can then be generated by DEA from the first component:

$$e^- + A \rightarrow A^{-\#} \rightarrow R_1 + X^- \quad (17)$$

which then undergoes the exchange reaction (16) with the "substrate" molecule RY, visible by the observation of the leaving group Y^-. Since the first step (reaction (17)) is generally *resonant* in nature, i.e., operative only within a particular energy range, observation of Y^- anions from a mixed cluster carrying the X^- resonance profile indicates that they are the result of the S_N2 reaction (16).

Here we study the specific reaction:

$$F^- + CH_3Cl \rightarrow [FCH_3Cl]^{\#-} \rightarrow CH_3F + Cl^- \quad (18)$$

and use NF_3 as source to generate the nucleophile F^-.

S_N2 reactions have played a significant role in the development of concepts in physical organic chemistry [63].

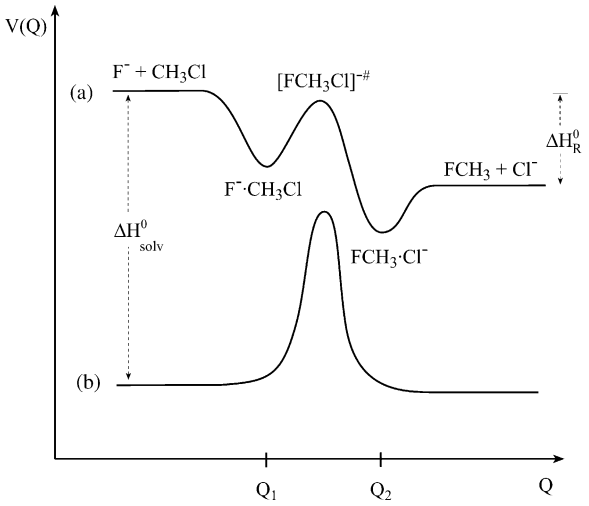

Fig. 14. Comparison of the potential energy surface in (a) the gas phase and (b) in the condensed phase along the reaction coordinate of the collinear S_N2 reaction $F^- + CH_3Cl \rightarrow CH_3F + Cl^-$.

While in solution educts and products are separated by an activation barrier (with its height largely controlled by the nature of the solvent), a gas phase S_N2 reaction proceeds through a double minimum potential (Fig. 14) as first suggested by Olmstead and Brauman [64]. The minima represent the ion–molecule complex before ($F^-{\cdot}CH_3Cl$) and after electron transfer and rearrangement of the (C–Cl) and the (C–F) bonds ($FCH_3{\cdot}Cl^-$).

It is well known that in the absence of solvation the rate constant can dramatically increase. For the system R = CH_3, X = Cl and Y = Br, for example, the gas phase rate constant ($2.1 \times 10^{-11}\,cm^3s^{-1}$) is by about 15 orders of magnitude (!) larger than that in water [16,65].

Gas phase S_N2 reactions have been studied since more than two decades. The experimental techniques include ion cyclotron resonance (ICR) mass spectrometry [64,66,67] high pressure mass spectrometry [68], flow or drift techniques [69–71] and recently also by guided ion beam tandem mass spectrometry [72].

The present system NF_3/CH_3Cl is of particular interest as the substrate molecule CH_3Cl has an extremely low cross section for dissociative electron attachment [73,74], i.e., Cl^- formation is below the detection limit of the present experimental device. On the other hand, NF_3 is an effective electron scavenger generating F^- in the energy range ≈0–4 eV [75]. As we shall demonstrate Cl^- ions are effectively produced via the title S_N2 reaction when CH_3Cl is weakly coupled to NF_3 molecules in a van der Waals cluster.

3.2.1.1. Electron attachment to the homogeneous components. CH_3Cl clusters. Before discussing reactions in binary NF_3/CH_3Cl [77] clusters we shall briefly recall the low energy attachment behavior of the two separated components. It is well known that within the chloromethanes the cross section for DEA increases strongly with the degree of

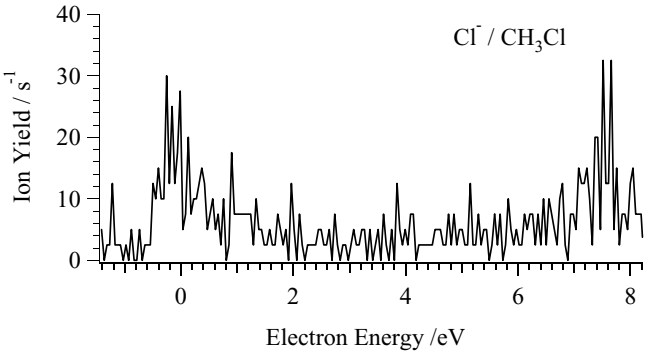

Fig. 15. Cl^- yield obtained from a pure CH_3Cl expansion seeded in Ar (1:10) at a stagnation pressure of 2 bar (adapted from Ref. [77]).

chlorination [2,76]. According to recent experimental and theoretical studies [73,74], the cross section for the low energy (<1 eV) DEA reaction:

$$e^- + CH_3Cl \rightarrow CH_3Cl^{-\#} \rightarrow CH_3 + Cl^- \quad (19)$$

is $\approx 5 \times 10^{-23}\,cm^2$ at room temperature, increasing with temperature and reaching $\approx 8 \times 10^{-20}\,cm^2$ at 600 K. This is orders of magnitude lower than that for the higher chlorinated methanes and, for example, about 10 orders of magnitude (!) lower than the DEA cross section in CCl_4 [5,78]. It thus appears that in earlier experiments any detected low energy Cl^- signal was due to impurities. The molecule possesses a second Cl^- DEA resonance located at 7.4 eV with an absolute DEA cross section of $\approx 5 \times 10^{-20}\,cm^2$ [73].

Fig. 15 shows the formation of Cl^- observed from a pure CH_3Cl expansion (seeded in Ar, 1:10) at a stagnation pressure of 2 bar yielding two weak signals near 0 and 7.4 eV.

The 7.4 eV signal can be assigned to DEA to CH_3Cl and eventually CH_3Cl clusters and the low energy signal to (probably very small) impurities in the sample and/or the gas inlet system. At a cross section of some $10^{-20}\,cm^2$ a count rate of a few tens of Cl^- ions per second is also expected from the given electron intensity, target gas pressure and detection efficiency of the present device. It should also be noted that the adiabatic expansion produces internally cold molecules, having a DEA cross section even lower than the value for room temperature given above. Under the present experimental conditions we thus expect at low energies a Cl^- count rate much below $1\,s^{-1}$ which is below the detection limit of the present experiment. The very small Cl^- impurity, however, does not affect any of the further results or conclusions. We mention that no parent anion CH_3Cl^- and no solvated fragment anions of the form $Cl^-{\cdot}(CH_3Cl)_n$ could be detected. According to recent ab initio calculations [74], the CH_3Cl^- potential energy curve does not possess a minimum which in turn means that methylchloride has *no positive adiabatic electron affinity*, i.e., the parent negative ion is thermodynamically unstable.

NF_3 clusters. The electron attachment behavior of NF_3 in the gas phase (single molecules and clusters [75]) and also in the condensed phase [79] has recently been studied in

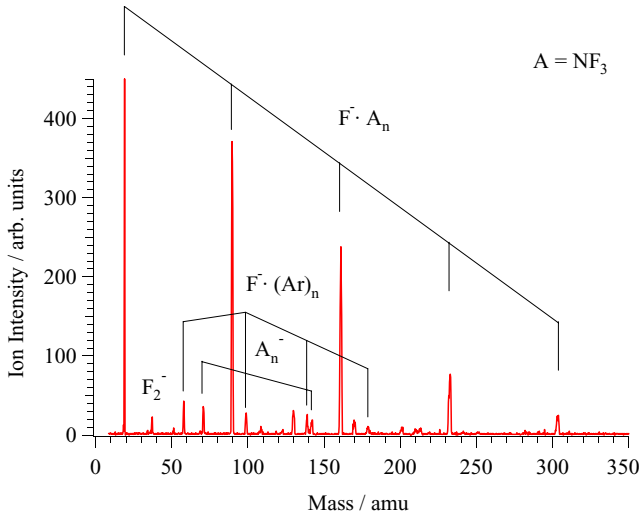

Fig. 16. Negative ion mass spectrum obtained from a pure NF_3 expansion seeded in Ar (1:50) at a stagnation pressure of 3 bar, recorded at an electron energy of 2 eV, A = NF_3. The peaks at 130, 170 and 210 amu can be assigned to the ternary complexes $F^-{\cdot}NF_3{\cdot}(Ar)_n$ (n = 1–3) (adapted from Ref. [77]).

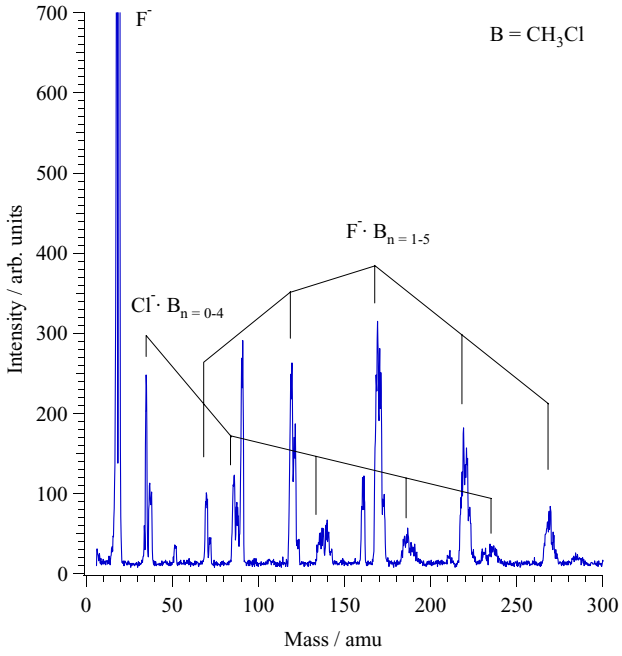

Fig. 17. Negative ion mass spectrum obtained from an expansion the a gas mixture NF_3/CH_3Cl/Ar (4:1:50) at a stagnation pressure of 3 bar recorded at 2 eV electron energy, B = CH_3Cl. For the assignment see also the text (adapted from Ref. [77]).

detail. The molecule possesses a broad resonance extending from ≈0–4 eV and peaking near 2 eV. Under collision free conditions the precursor ion dissociates predominantly into the fragments $F^- + NF_2$. The two comparatively weaker (<3%) dissociation channels $F_2^- + NF$ and $NF_2^- + F$ are also observed. The absolute DEA cross section at the resonance maximum is near 10^{-17} cm^2. TOF experiments in the gas phase [75] indicate that the broad feature between ≈0 and 4 eV consists of two overlapping resonances, with the first one associated with the electronic ground state and decomposing into F^- with appreciable kinetic energy.

Electron attachment to a beam of neutral NF_3 clusters generates (in addition to the DEA fragments observed from single molecules) the stabilized parent molecular anion $NF_3{}^-$, the higher homologues $(NF_3)_n{}^-$ and the solvated fragment ions $F^-{\cdot}(NF_3)_n$, all formed within the prominent DEA resonance peaking near 2 eV, subjected to some minor energy shift of the resonance position due to solvation and some energy dependence in the decomposition of the precursor cluster into the particular channel. In Fig. 16 the negative ion mass spectrum is shown obtained from a pure NF_3 expansion seeded in Ar (1:50) at a stagnation pressure of 3 bar and recorded at an electron energy of 2 eV (for the ion yield curves see the next section). The "naked" DEA fragments (F^-, $F_2{}^-$, $NF_2{}^-$) as well as the homologous series $A_n{}^-$, n = 1, 2 (A = NF_3) and $F^-{\cdot}A_n$ (n = 1–4) can clearly be seen. There is also evidence for the formation of $F^-{\cdot}Ar_n$ (n = 1–3) clusters and the ternary complexes $F^-{\cdot}NF_3{\cdot}(Ar)_n{\cdot}$($n$ = 1–3) at 130, 170 and 210 amu, respectively. Interestingly, the intensity of the solvated ions $F^-{\cdot}A_n$ is about one order of magnitude larger than that of the stoichiometric complexes $(NF_3)_n{}^-$. This can be rationalized by the amount of excess energy to be dissipated: once the transient ion $NF_3{}^-$ is formed via a Franck-Condon transition within the target cluster, formation of the relaxed ion $NF_3{}^-$ requires dissipation of considerably more energy than generation of the DEA fragment F^-. This is a consequence of the appreciable electron affinity of NF_3 (1.7 eV [75]) compared to the thermodynamic threshold for F^- formation (−0.76 eV). In terms of a more microscopic description, once the precursor ion is formed in its repulsive state within the target cluster, in the very first step dissociation into the DEA fragments $F^- + NF_2$ is more likely than relaxation into the potential minimum of the $NF_3{}^-$surface.

3.2.1.2. S_N2 reactions in mixed NF_3/CH_3Cl clusters. Fig. 17 presents the negative ion mass spectrum obtained from electron attachment to the neutral cluster beam produced by adiabatic expansion of the NF_3/CH_3/Ar gas mixture (4:1:50) at a stagnation pressure of 3 bar and an electron energy of 2 eV. The mass spectrum is now much more complex than that from the pure NF_3 expansion and the peaks are considerably broader, mainly due to the unresolved ^{35}Cl and ^{37}Cl isotopes. In addition, we are now faced with the problem of *mass coincidences*, i.e., chemically different complexes having the same mass number. Moreover, even complexes with a given (stoichiometric) composition may belong to chemically different species.

The composition of the neutral beam is not exactly known, it definitely consists of mixed clusters (see below), it may also contain homogeneous clusters as well as monomers. There is also some background level of monomers in the collision chamber due to scattered gas from the molecular beam.

In the mass spectrum of Fig. 17 we can identify (a) the naked DEA products from A (A = NF_3) F^-, $F_2{}^-$, and $NF_2{}^-$ arising either from monomers or clusters, (b) the series $F^-{\cdot}A_n$ like in the pure expansion, (c) complexes of the form $F^-{\cdot}B_n$ (B = CH_3Cl) ($n = 1$–6) and $A^-{\cdot}B_n$ ($n = 1$–4) and $F^-{\cdot}A{\cdot}B_n$ ($n = 1, 2$) which must arise from reactions in mixed clusters, and (d) most important, the "naked" leaving group Cl^- and complexes of the form $Cl^-{\cdot}B_n$ ($n = 1$–5) containing the dissociation product Cl^-. Since the component B = CH_3Cl does not yield any Cl^-, these latter ions must be products of a completed S_N2 reaction in a mixed cluster. For both the observed Cl^- ion and the ion complexes we can definitely exclude that they are the result of a reaction between uncorrelated monomers: effusing the gas mixture into the reaction volume through the capillary does not yield any detectable signal of Cl^- or of the ionic complexes from above, even when increasing the pressure into the 10^{-4} mbar range. In this case we only detect the naked DEA products from NF_3.

Concerning the problem of mass coincidences mentioned above, the series $A^-{\cdot}B_n$ partly overlaps with the series $F^-{\cdot}B_{n+1}$ as, for example, the mass of $F^-{\cdot}(CH_3{}^{35}Cl)_n{\cdot}(CH_3{}^{37}Cl)$ coincides with that of $NF_3{}^-{\cdot}(CH_3{}^{35}Cl)_n$ (mass number 121). Localization of the excess charge in the assignments of Fig. 17 is usually unambiguous due to the large electron affinity differences of the constituents of the particular complex. For the complex $F^-{\cdot}CH_3Cl(F^-{\cdot}B)$, however, we are faced to the abovementioned problem of the chemical identity for a given stoichiometric composition: in the course of a collinear bimolecular reaction it can be the stabilized ion–molecule complex either *before*, $F^-{\cdot}CH_3Cl$ or *after* completion of the reaction, $FCH_3{\cdot}Cl^-$. Accordingly, for the larger compounds which in Fig. 17 we have assigned as $F^-{\cdot}B_n$ we cannot conclude from mass spectrometry alone whether it is $F^-{\cdot}(CH_3Cl)_n$ or $Cl^-{\cdot}(CH_3F){\cdot}(CH_3Cl)_{n-1}$. Note that complexes of the form $Cl^-{\cdot}B_n$ now appear (in contrast to the pure CH_3Cl expansion), but no complexes of the form $Cl^-{\cdot}A_n$.

In Figs. 18 and 19 we present the explicit energy dependence of the yield of some selected ions obtained under comparable experimental conditions as the mass spectrum of Fig. 17.

The energy dependence of the F^- yield (Fig. 18a) essentially resembles that from a pure NF_3 expansion. This signal can be the result of DEA to (i) some NF_3 containing cluster, (ii) NF_3 monomers traveling in the beam, or (iii) NF_3 in the background gas. Fig. 18b, on the other hand, demonstrates that Cl^- is now effectively produced with an energy dependence roughly resembling that of F^- which is a further indication that it is in fact the result of an S_N2 reaction in a mixed cluster. A closer inspection of Fig. 18, however, reveals that the Cl^- resonance profile (and also that of $Cl^-{\cdot}CH_3Cl$, Fig. 18c) is subjected to some shift to lower energy.

Fig. 19 shows the energy dependence of three further ions. In 19a it is $F^-{\cdot}CH_3Cl$ which is probably a mixture of the ion molecule complex before, $F^-{\cdot}CH_3Cl$, or after completion of the reaction, $FCH_3{\cdot}Cl^-$. The solvated ion $F^-{\cdot}NF_3$ is definitely the result of DEA to NF_3 in a cluster with an energy dependence closely resembling that of F^-, i.e., with some shift to higher energy compared to the S_N2 product ions Cl^- and $Cl^-{\cdot}CH_3Cl$, and 19c shows the DEA product $NF_2{}^-$.

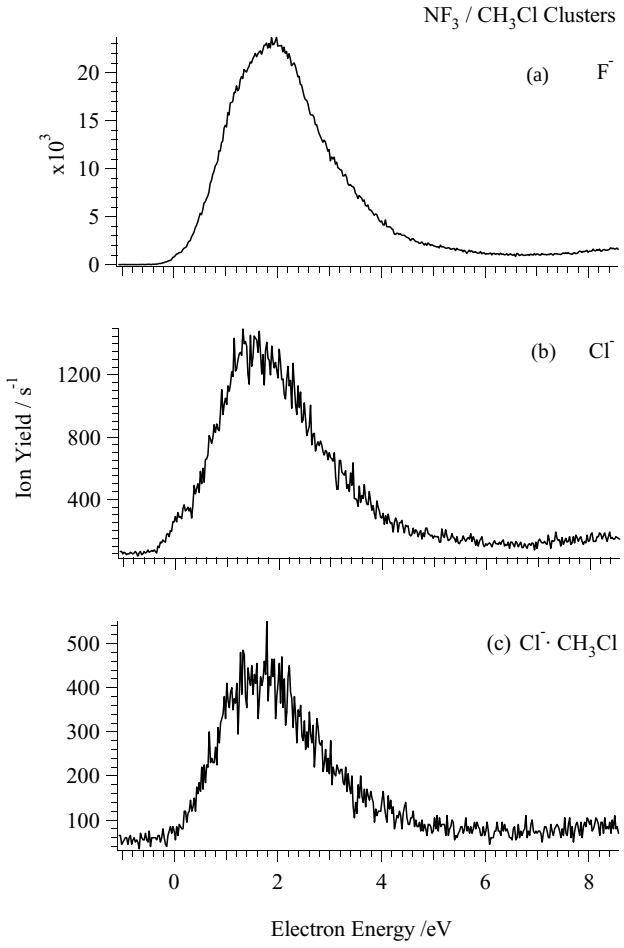

Fig. 18. Energy profile of the nucleophile F^-, the leaving group Cl^- and the ion molecule complex $Cl^-{\cdot}CH_3Cl$ observed from a mixed expansion under the conditions of the negative ion mass spectrum in Fig. 16.

From the well established bond dissociation energies $D(CH_3–Cl) = 3.62$ eV, $D(CH_3–F) = 4.89$ eV and electron affinities $EA(Cl) = 3.61$ eV, $EA(F) = 3.40$ eV [39] the reaction enthalpy for the title S_N2 reaction becomes -1.48 eV. Further, the thermodynamic threshold for the DEA reaction in NF_3 for F^- formation is -0.76 eV. Thus, by scanning over the resonance energy from about 0 to 4 eV one increases the *total excess energy* for the gas phase S_N2 reaction from more than 2 eV to more than 6 eV.

3.2.2. Energy dependence of S_N2 reaction efficiency

In a variable-temperature-selected ion flow drift tube experiment [80] it was shown that the gas phase reaction rate is only weakly sensitive on the temperature of the substrate molecule. The constant decreases moderately from 1×10^{-9}

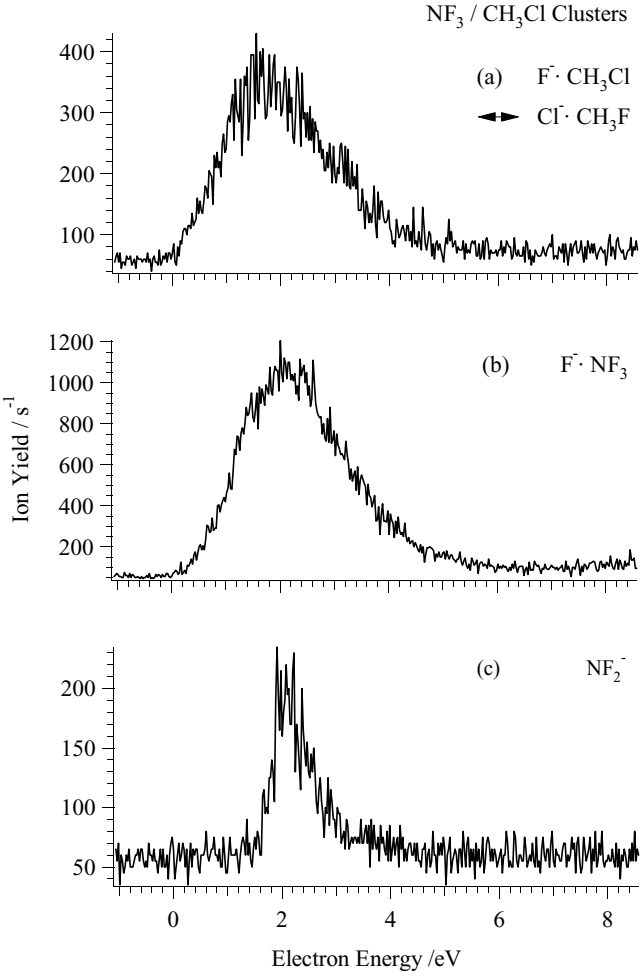

Fig. 19. Energy profile of some selected products recorded under the conditions of the negative ion mass spectrum (Fig. 16). The complex assigned as $F^-{\cdot}CH_3Cl$ is most likely a mixture between $F^-{\cdot}CH_3Cl$ and $FCH_3{\cdot}Cl^-$ (see the text).

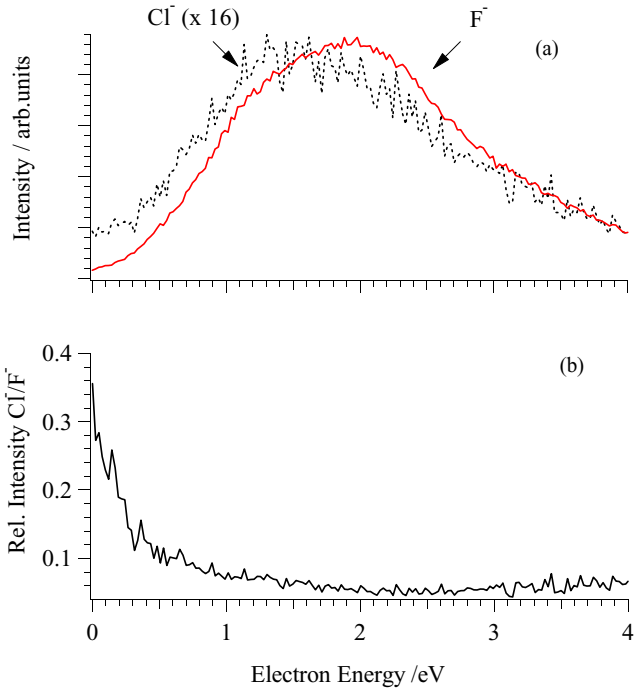

Fig. 20. (a) Comparison of the energy profile of the nucleophile (F^-) with the naked product ion (Cl^-) and (b) energy dependence of the ratio Cl^-/F^-.

to 2×10^{-10} cm^3 s^{-1} on increasing the (center of mass) collision energy from 0.3 to 1 eV as expected for an exothermic reaction.

Returning to the ion yields in Fig. 18 it is obvious that on the low energy side of the resonance region the leaving group Cl^- is preferentially formed over F^-. In Fig. 20a we have directly plotted the comparison between the two yields and in 20b the ratio Cl^-/F^- indicating that this ratio drops by a factor of about 4 between ≈0 and 1.5 eV and remains virtually constant above that energy. Superficially one might be tempted to use this ratio as a mirror of the reaction efficiency as a function of the *total available excess energy* under the particular conditions. These conditions are, for example, defined by the initially DEA step creating the nucleophile with a given amount of translational energy. As mentioned above, from the gas phase experiments we know that the broad DEA resonance consists of two different electronic states releasing the *kinetic energy* in a different way.

However, one has to be careful when extracting information from the energy dependence of the Cl^-/F^- ratio for the following reasons: (i) by considering the ratio Cl^-/F^- alone one compares the free DEA product F^- with the naked leaving group. In actual practice, the energy dependence of the nucleophile initiating an S_N2 reaction *in a cluster* may differ to some extend to that recorded in Fig. 20 which represents *a free* ion resulting from DEA to a clusters or an isolated molecule, (ii) accordingly a completed S_N2 reaction is not only mirrored by the naked leaving group but also through their various ion molecule complexes. Some of them cannot be identified by mass spectrometry alone as they may represent the complex before or after the reaction (supra vide). We hence conclude that the decreasing value for the ratio Cl^-/F qualitatively reflects the decreasing reaction efficiency in the cluster by increasing the total excess energy.

In conclusion from the present results it can be seen that low energy (<4 eV) electron interaction with CH_3Cl (single molecules and clusters) does not result in a measurable negative ion signal. In contrast to that, from mixed clusters containing NF_3 and CH_3Cl the fragment ion Cl^- and complexes containing Cl^- are effectively produced via the S_N2 reaction (18).

3.3. Condensed and adsorbed molecule

In this last section we shall illustrate the behavior of negative ion resonances on surfaces for a few prototypical case studies. The results will be discussed on the background of

the intrinsic properties of the corresponding gas phase analogues. A powerful technique to study negative ion resonances at surfaces is ESD of negative ion fragments, a field which has been pioneered by Sanche one and a half decade ago [81,82]. Electron stimulated reactions at the surface or in the bulk can directly be followed by the infrared reflexion absorption spectroscopy (IRRAS) which probes vibrations of the molecules in the adsorbate. For the present examples we shall focus on (ESD) of negative ions. We start with an example demonstrating how the stage of aggregation affects the DEA process by going from single molecules over clusters to surfaces of nanofilms.

3.3.1. The effect of aggregation in dissociative electron attachment to SF_5CF_3

The molecule trifluoromethylsulphur pentafluoride (SF_5CF_3) is a more or less arbitrarily chosen compound to demonstrate the effect of a surrounding medium. The molecule has been recently discovered in stratospheric air at concentrations of about 0.12 ppt. It is of anthropogenic origin, its sources, however, are yet not clearly identified [83]. SF_5CF_3 possesses several strong IR bands in the "atmospheric IR window" (800–1300 cm^{-1}) and is considered the most effective greenhouse gas on a per molecule basis in the Earth's atmosphere [83].

3.3.1.1. Single collision conditions. Fig. 21 shows negative ion yields obtained from gas phase SF_5CF_3 under single collision conditions in the energy range 0.0–5 eV. Only *fragment* ions are observed appearing from pronounced resonance features reminiscent of DEA. By far the most dominant channel is the formation of SF_5^- from a very intense resonance peaking near 0 eV and extending to about 2 eV. Further much weaker DEA channels produce CF_3^- and F^- in agreement with another gas phase experiment [84]. An earlier study [85] on the total attachment cross section (no mass identification) reported a strong signal at low energies and two further comparatively weak resonances peaking near

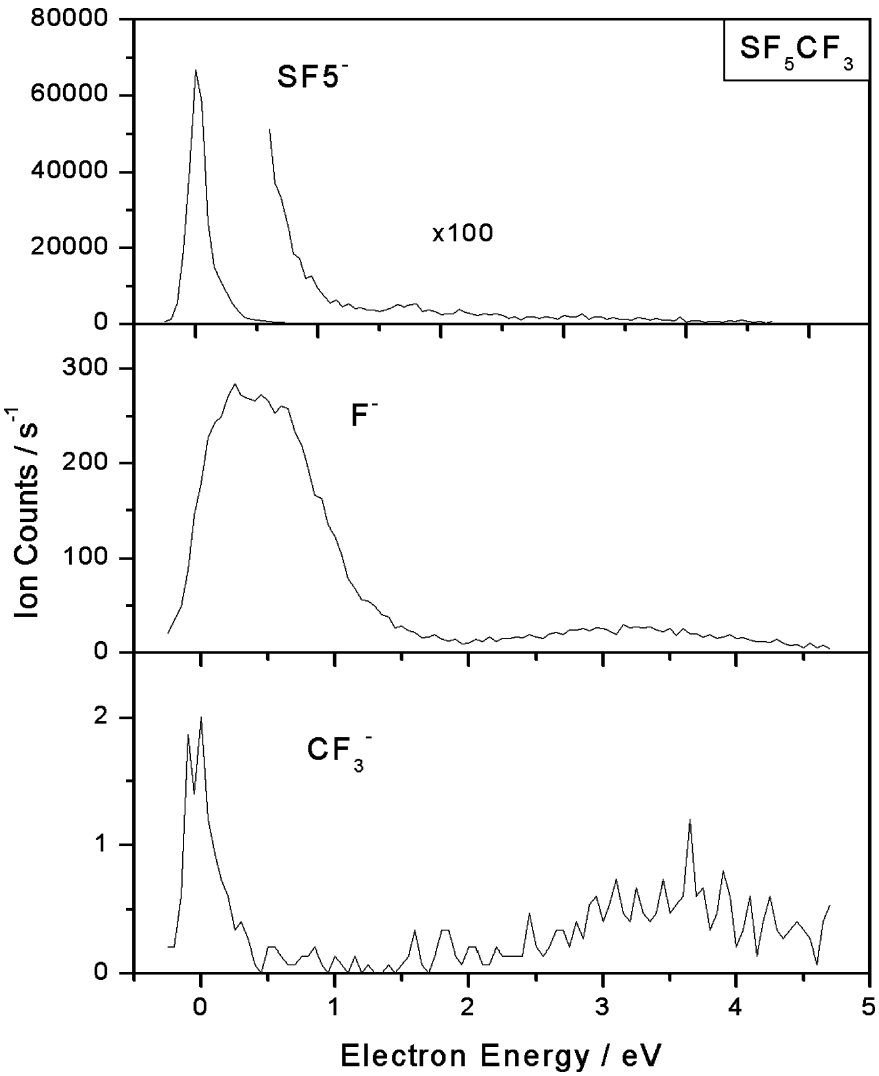

Fig. 21. Formation of SF_5^-, F^- and CF_3^- from SF_5CF_3 as a function of the electron energy in the range 0–5 eV under single collision conditions. Pressure of the gas 3×10^{-6} mbar measured at the ionization gauge. Count rates in absolute units (adapted from Ref. [86]).

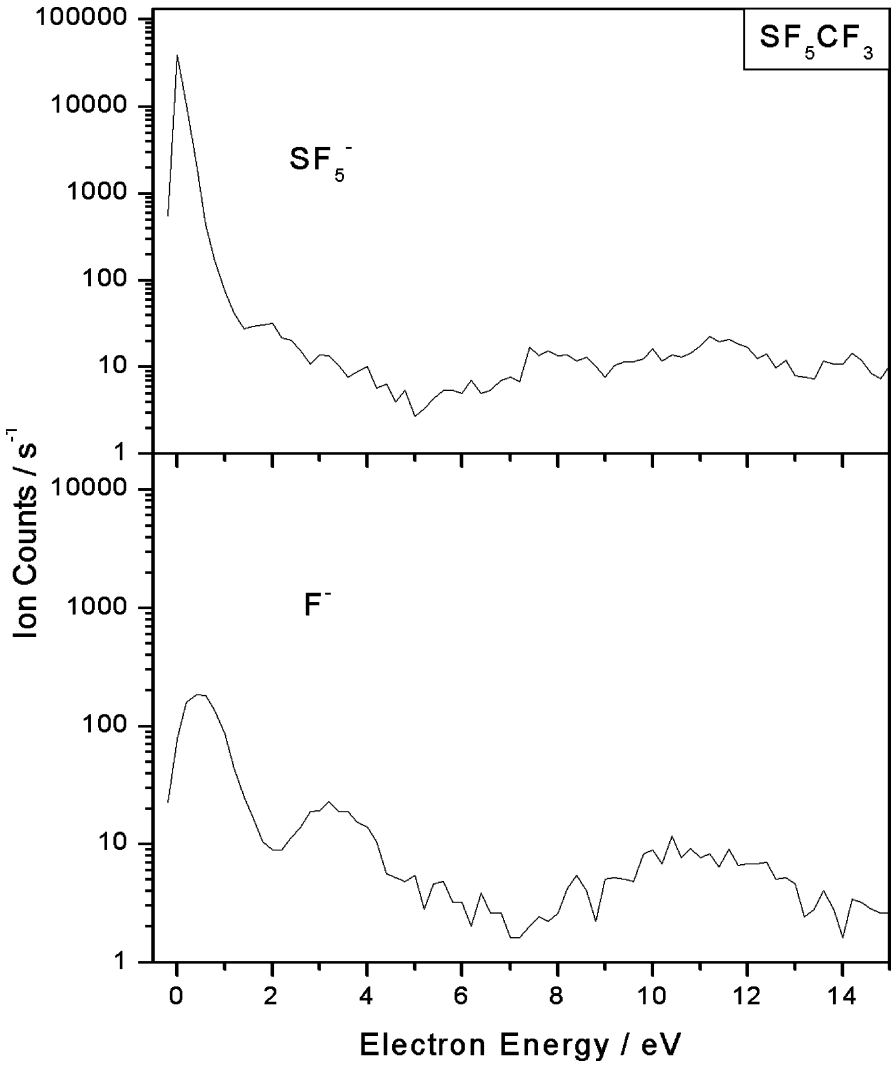

Fig. 22. Formation of SF_5^- and F^- from SF_5CF_3 in the extended energy range 0–15 eV on a log intensity scale (adapted from Ref. [86]).

3.5 and 11 eV. As can be seen from the logarithmic intensity representation extending to 15 eV (Fig. 22), these higher energy features are also visible in the F^- DEA channel.

For the gas phase we can conclude that electron attachment is strongly dominated by the SF_5^- channel due to the DEA reaction:

$$e^- + SF_5CF_3 \rightarrow SF_5CF_3^{\#-} \rightarrow SF_5^- + CF_3 \quad (20)$$

The absolute cross section reaches values near 1×10^{-14} cm^2 at energies approaching 0 eV [84,85]. On the basis of established thermochemical values, process (20) is exothermic by −0.30 eV. In electron attachment to SF_5CF_3 under collision free conditions, we do not observe any undissociated anion $SF_5CF_3^-$ within the time scale of the experiment (≈50 μs).

3.3.1.2. SF_5CF_3 clusters. Adiabatic expansion of SF_5CF_3 diluted in Ar leads to molecular aggregates including mixed SF_5CF_3/Ar clusters as can be seen, for example, by the negative ion mass spectrum (Fig. 23), recorded at an impact energy close to 0 eV. The cluster beam was generated by adiabatic expansion of an SF_5CF_3/Ar gas mixture at a ratio of 1:1000 and a stagnation pressure of 3 bar. In the mass spectrum the peak in the range 196–198 amu can be assigned to the undissociated parent negative ion indicating that SF_5CF_3 possesses a positive adiabatic electron affinity. The structure of all mass peaks is due to the isotopes ^{32}S, ^{33}S, ^{34}S with the relative abundances of 95:0.8:4.2. The strongest signal in the mass spectrum is still SF_5^-, it has to be kept in mind, however, that this signal can arise from both, electron attachment to clusters and to monomers (background gas and monomers traveling in the molecular beam). On the other hand, negative ions observed at mass numbers higher than the parent molecule must arise from reactions occurring in a cluster. Apart from SF_5^- and $SF_5CF_3^-$ we observe in the mass range up to 300 amu the solvated fragment ions $Ar_n \cdot SF_5^-$ (n = 1, 2) and complexes of the form $Ar_n \cdot SF_5CF_3^-$ (n = 0–3) containing the undissociated negative parent anion. The mass spectrum also contains an SF_6^- signal from the calibration gas.

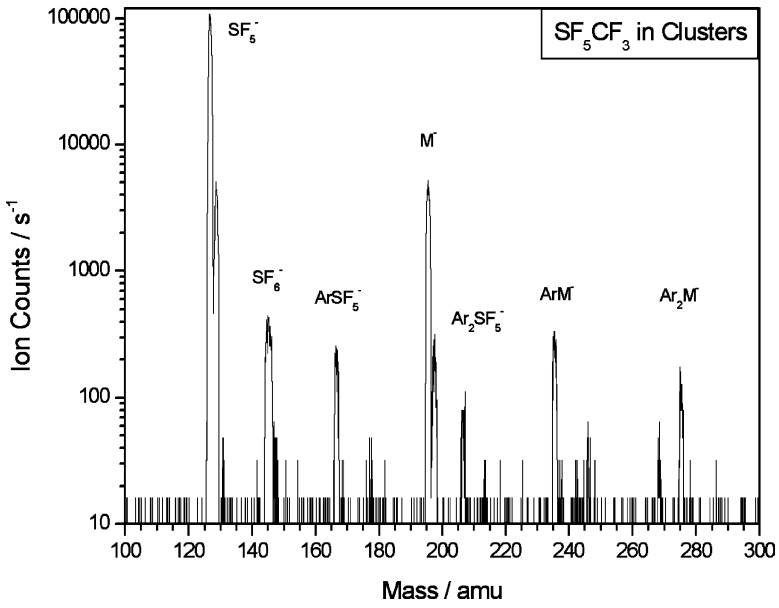

Fig. 23. Mass spectrum of negative ions from an expansion of SF_5CF_3 seeded in Ar (1:1000) at 3 bar and an electron energy close to 0 eV, M = SF_5CF_3. The structure of the mass peaks is due to the isotopes ^{32}S, ^{33}S, ^{34}S (see the text).

Formation of the parent negative ion is due to evaporative attachment, i.e., resonant capture of an electron by a cluster thereby generating an individual TNI within the target aggregate:

$$e^- + (SF_5CF_3)_m \cdot Ar_n \rightarrow SF_5CF_3^{\#-} \cdot (SF_5CF_3)_{m-1} \cdot Ar_n \quad (21a)$$

which then decomposes. Since this reaction occurs close to 0 eV, the excess energy is essentially comprised of the electron affinity of SF_5CF_3 which is used to evaporate the cluster according to:

$$SF_5CF_3^{\#-} \cdot (SF_5CF_3)_{m-1} \cdot Ar_n \rightarrow SF_5CF_3^- + (m-1)SF_5CF_3 + nAr \quad (21b)$$

In (21b) it is assumed that the initial aggregate completely evaporates into monomers.

Formation of the undissociated parent anion $SF_5CF_3^-$ in electron attachment to clusters indicates that the reactivity of the target molecule is suppressed to some degree under aggregation, i.e., a fraction of attachment events is channeled into nondissociative processes. We can give a lower limit for the branching ratio between associative and dissociative processes by assuming that the SF_5^- signal completely arises from clusters. In this case we obtain a lower limit for the branching ratio as AA/DEA $\geq$ 5%, where AA assigns associative attachment leading to undissociated product ions.

Fig. 24 shows explicit ion yield curves on a log scale for the products SF_5^-, $SF_5CF_3^-$, and F^- from electron attachment to clusters. As expected, formation of the undissociated parent anion is concentrated in the low energy domain with a peak width broader than that from the calibration compound SF_6^-. Interestingly, from clusters one observes a surprisingly strong low energy SF_5^- signal and considerable enhancement in the energy range of the second resonance feature. From gas phase molecules this resonance is only very weak on the SF_5^- channel, but clearly visible on the F^- yield (Fig. 21) and also the total attachment cross section [85]. In clusters this second resonance is clearly visible on the SF_5^- channel now peaking slightly below 3 eV. This shift principally mirrors the solvation energy of the TNI in the clusters. More precisely, the peak position of an ionic product is a convolution of the energy of the precursor ion (due to the initial Franck-Condon transition) convoluted with the energy dependent probability to decay into the channel under observation. The solvation shift can hence be counterbalanced to some degree by the energetics of the decomposition. On the F^- channel (Fig. 24) this second feature is still weakly present near 3.5 eV.

On the basis of the high dilution of SF_5CF_3 in the carrier gas, the strong signal on the SF_5^- channel is very striking and points towards an enhancement in low energy DEA. Since we do not have direct access to the actual pressure in the collision region, it is impossible to extract absolute cross section. The usual observation, however, is that the signal from electron attachment to the cluster beam is about one order of magnitude weaker compared to the effusive beam. Such a ratio is in fact observed on the F^- count rates (Figs. 21 and 24) and supports the picture of a *medium enhancement* particularly on the SF_5^- fragment.

3.3.1.3. Desorption of negative ions from condensed SF_5CF_3. Fig. 25 shows negative ion desorption from an eight monolayer (ML) film of SF_5CF_3 directly condensed onto the Au surface. A remarkably strong F^- desorption signal is observed peaking at 11 eV and there is also a com-

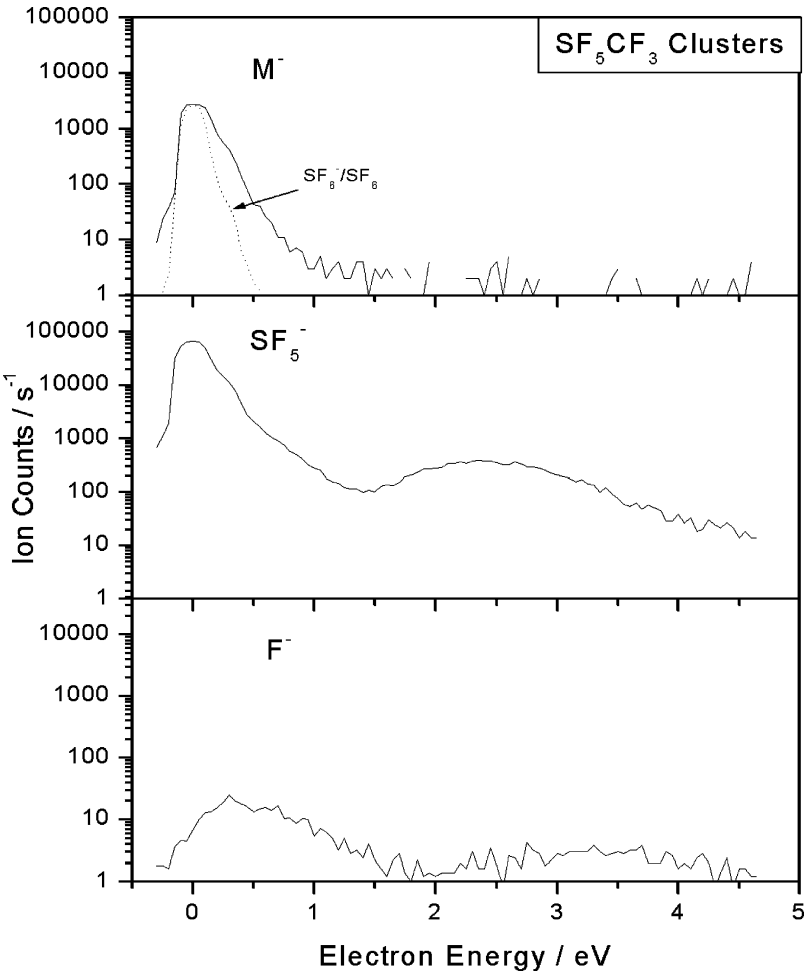

Fig. 24. Explicit ion yields for the stabilized parent anion $SF_5CF_3^-$ and the fragments SF_5^- and F^- on a log intensity scale from electron attachment to clusters under the conditions of Fig. 23 (adapted from Ref. [86]).

paratively weak F_2^- yield appearing at still higher energies. These two ions are the only negatively charged desorption products observed from SF_5CF_3. F^- appears within an intense resonance due to DEA at the surface followed by desorption of the fragment ion. In the gas phase the DEA cross section shows a small structure near 11 eV on both F^- and SF_5^- which is, however, weak compared to the dominant low energy DEA process generating SF_5^-. We have thus a situation where the *gas phase* molecule is effectively decomposed by low energy electrons while in the condensed phase the ion desorption channel is completely suppressed at these energies. In turn, desorption is very effective at 11 eV where gas phase DEA is comparatively weak. From the nonobservation of an ion desorption signal at low energies, however, it does not necessary follow that the DEA reaction at the surface is completely suppressed in that energy range. It may still be operative with dissociation products remaining at the surface. Desorption experiments on H_2O layers and also on solid Ar did not indicate any appreciable suppression of the desorption yield indicating that F^- is formed in a rather impulsive reaction with considerable excess energy on F^- [86].

The present desorption experiment demonstrates that features barely seen in the gas phase (F^- near 11 eV) can become very pronounced in desorption. In the following we shall discuss possible medium enhancements in DEA more generally.

3.3.2. Medium enhanced dissociative electron attachment

Any environment, in particular a surface provides effective means to dissipate energy via intermolecular collisions. For a NIR at a surface one would consequently expect a considerable decrease in the reactivity (bond cleavage via DEA) in favour of associative attachment yielding undissociated anions. This is in fact the observation in many systems. In C_6F_5I, for example, solvation switches the process quantitatively from dissociative attachment (single molecules) to associative attachment (clusters) [87]. There are, however, also mechanisms where the medium can *enhance* DEA.

The mechanism for such an enhancement is based on the effect of the medium on autodetachment rate, i.e., the lifetime of the resonance towards energy loss. Any change in the rate must be counterbalanced by the two competing reactions associative or dissociative electron attachment. Both

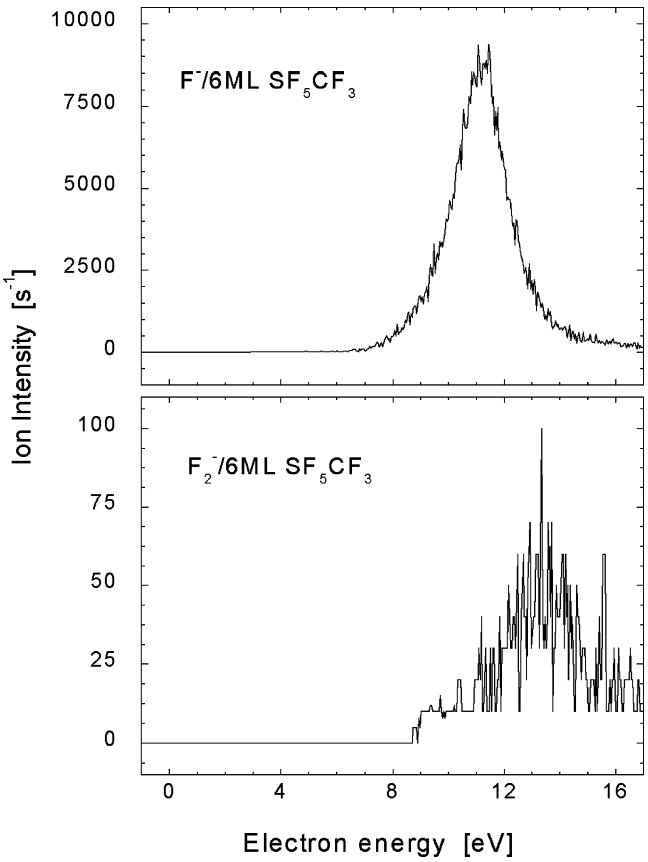

Fig. 25. Desorption of F^- and F_2^- from an 8 ML film of SF_5CF_3 condensed directly on the metallic substrate at 40 K (adapted from Ref. [86]).

keep the additional electron in a bound state within the system.

In the case of CF_4 (where the two DEA channels yielding $F^- + CF_3$ and $F + CF_3^-$ are operative along repulsive potential energy surfaces) charge trapping experiments demonstrate [88] that the cross section for DEA is increased by a factor of 4–7 when going from gas phase molecules to a multilayer CF_4 film. A considerably larger enhancement (6 (!) orders of magnitude) has been estimated for CH_3Cl [89]. The enhancement can be illustrated by means of a two dimensional potential energy curve (Fig. 26). V_i denotes the initial state (neutral molecule) and V_f the final state (negative ion). The dotted curves represent the corresponding states in a medium with the ionic state much more affected due to polarization. According to Heisenberg's uncertainty relation the energy width $\Gamma(R)$ of the ionic state mirrors the lifetime with respect to autodetachment. From Fig. 26 it is immediately clear that in the solvated system the time the dissociating system spends in the area *active* for autodetachment ($R < R_{c,ad}$) is reduced and therefore electron loss is decreased in favour of dissociation. The effect is the more pronounced the larger the autodetachment width is. Fig. 26 describes DEA involving the electronic ground state of the anion where dissociation occurs along the lowest potential energy surface with no curve crossings.

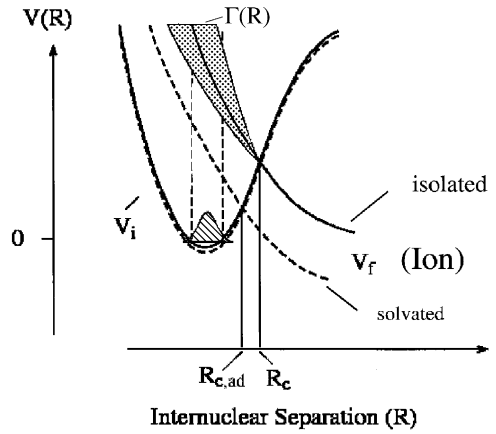

Fig. 26. Dissociative electron attachment along a repulsive surface illustrating the effect of a medium on the DEA cross section. The dotted curves represent the system in the condensed phase. $\Gamma(R)$ is the energy width of the ionic state due to autodetachment. The time for dissociation in the area active for autodetachment is shortened in the condensed phase.

A second mechanism refers to electronically excited states where also appreciable enhancements are observed [90]. One of the many examples is shown in Fig. 27 in the case of DEA to CHF_2Cl [91]. In the gas phase this molecule generates Cl^-, F^- and H^- ions. The most abundant channel is Cl^- (Fig. 27a) with an estimated cross section in the range of a few 10^{-20} m^2 at thermal electron energies. There are further weak resonant structures seen at higher energies which are due to core excited resonances.

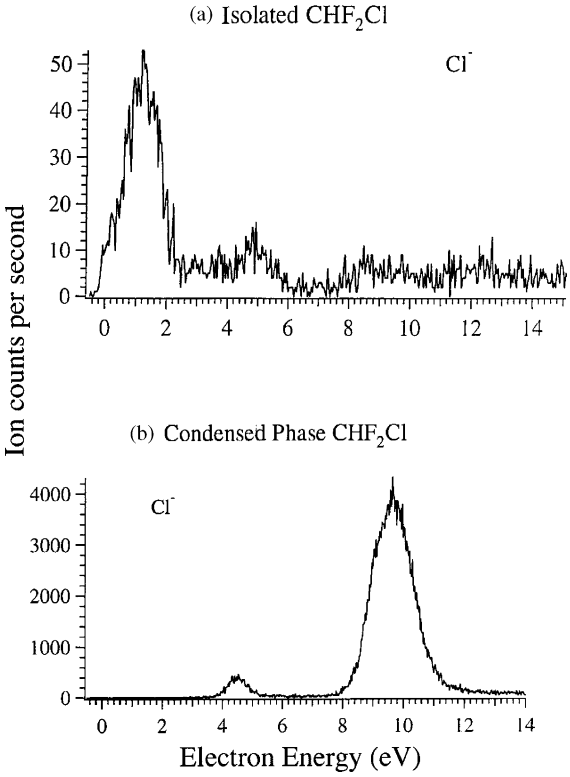

Fig. 27. Comparison of the Cl^- yield from isolated CHF_2Cl and from a two layer CHF_2Cl film.

Desorption of Cl^- from a two layer CHF_2Cl film condensed directly on the metallic substrate, on the other hand, shows an appreciable signal in the Cl^- desorption yield. While the low energy resonance seen in the gas phase DEA spectrum is completely suppressed in the Cl^- desorption spectrum, two resonances peaking at 4.2 and 9.8 eV appear in the desorption signal. In the gas phase the lowest DEA channel:

$$e^- + CHF_2Cl \rightarrow CHF_2 + Cl^- \quad (22)$$

is approximately thermoneutral ($\Delta H_o \approx 0$ eV). The energetic threshold for desorption of an ion ($\Delta H_{o,d}$) from a molecular film can be approximated by:

$$\Delta H_{o,d} = \Delta H_o + \frac{m_i}{m} V_p \quad (23)$$

with m_i the mass of the ion, m that of the neutral fragment and V_p the polarization energy. If we take $V_p = 1$ eV as a reasonable value [91] for the threshold for Cl desorption becomes $\Delta H_{o,d} = 0.7$ eV. The observation that desorption is quantitatively suppressed below ≈3 eV reflects the fact that the kinetic energy imparted to Cl^- is insufficient to overcome the polarization potential. An unfavorable orientation of the molecule at the surface may additionally contribute to the lack of any desorption signal. In any case near 10 eV we observe an intense desorption signal where the gas phase DEA spectrum only yields a spurious contribution. A quantitative estimation of the absolute desorption cross section (taking into account the density of the molecules at the surface, etc.) leads to a value which is two orders of magnitude higher than the gas phase DEA cross section. It has to be noted that this number refers to the desorption cross section and does not include those DEA reactions leading to Cl^- fragments which remain at the surface. The above number is therefore a lower limit of the enhancement.

What is the mechanism for such a dramatic effect? For a core excited resonance it may no longer be adequate to describe its decay by the competition between dissociation and autodetachment along repulsive potential energy surfaces as in Fig. 26. At those energies the appreciable density of electronic states leads to many curve crossings and hence direct electronic dissociation processes are an exception. In addition the autodetachment lifetime depends strongly on the character of the core exited state. An *open channel* resonance is located in energy *above* the associated electronically excited state of the neutral and can effectively decay via one electron transitions into the associated neutral molecule. A *closed channel* (or Feshbach) resonance is located *below* the excited neutral and can only decay into the neutral molecule via a two electron process. Therefore Feshbach-type resonances have much longer autodetachment lifetimes. With respect to solvation this means that an open channel resonance in the gas phase can be converted into a Feshbach-type resonance in an environment. The increased autodetachment lifetime will result in an enhancement of the DEA cross section. This simple picture does not include any microscopic considerations in terms of the many possible potential energy surfaces. It simply describes the enhancement of the DEA cross section by the general possibility to switch between the character of the resonance with the associated different autodetachment lifetime. Fig. 28 illustrates the situation schematically in an energy diagram. The vertical arrows on the left side (open channel resonance) describe effective autodetachment via the one electron process.

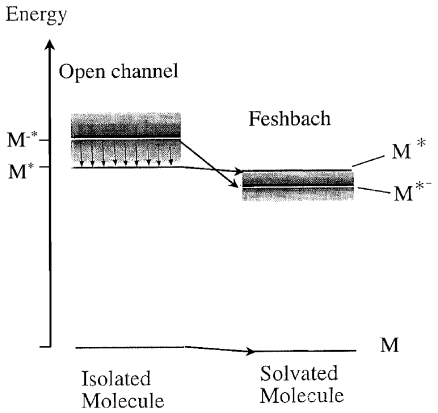

Fig. 28. Conversion of an open channel core excited resonance into a Feshbach-type resonance under solvation. The vertical arrows indicate effective autodetachment (one electron transitions) into the associated electronically excited neutral molecule.

3.3.3. Controlled surface modification by low energy electrons

In this case study we demonstrate an electron initiated reaction in the condensed phase in which the extend of a reaction can be pushed virtually completely onto the product side.

As shown above in many molecules dissociative electron attachment can be used as a tool to induce a completely selective bond cleavage. The selectivity is then simply due to energetics. We use this selectivity to drive an electron initiated reaction, which, by the choice of the electron energy, transforms the surface of a molecular film consisting of 1,2-$C_2F_4Cl_2$ molecules quantitatively into Cl_2 and (possibly polymerized) C_2F_4. While the transformation of the adduct 1,2-$C_2F_4Cl_2$ into Cl_2 can be followed by ESD [92], the byproduct (C_2F_4 and possibly Cl^- ions) is not yet identified experimentally.

Fig. 29 (top) shows Cl^- formation from condensed 1,2-$C_2F_4Cl_2$ as observed from the first scan within a newly deposited film of 5 ML. In the gas phase [93] Cl^- is exclusively formed at low energies (<1 eV, selective bond cleavage, not shown here) with an estimated DEA cross section of $(2 \pm 1) \times 10^{-15}$ cm^2. There is additional comparatively little Cl^- intensity from a resonant feature in the range 8–10 eV. In the desorption yield the intensity is reversed, comparable to the situation in CHF_2Cl described above. In the gas phase there are further DEA reactions on a comparatively weaker scale associated with the ions F^-,

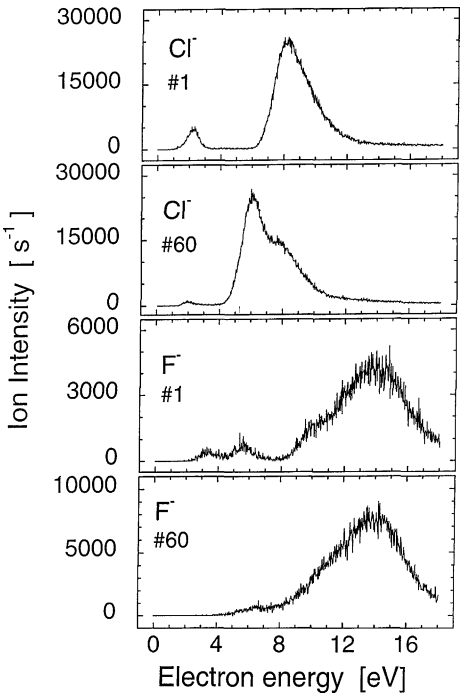

Fig. 29. Cl^- and F^- desorption signal from a 6 ML $C_2F_4Cl_2$ film before and after electron irradiation. First scan (#1) and 60th scan (#60) in the course of successive scans of 30 s scan time at a beam intensity of ≈100 nA (adapted from Ref. [92]).

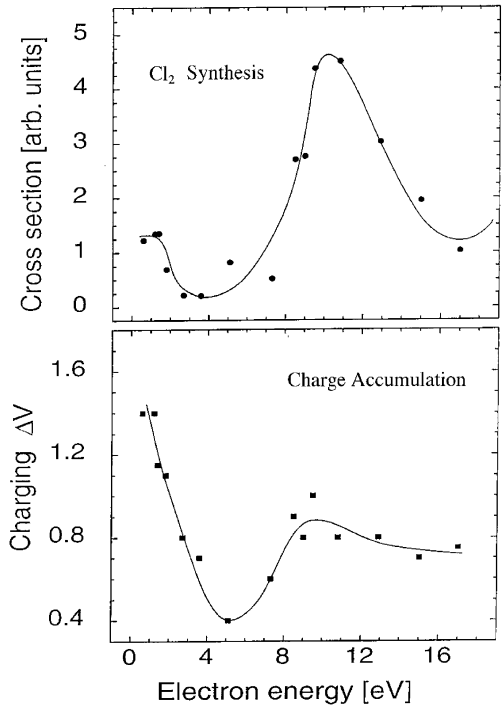

Fig. 30. Energy dependence of the relative cross section for Cl_2 formation. The numbers represent the peak area of the contribution near 6 eV assigned to Cl^-/Cl_2 after irradiation for 120 s each time (top); shift of the onset of the electron injection curve (ΔV) with respect to the monochromator potential after 120 s irradiation. ΔV is a measure of the charge accumulated in the film (adapted from Ref. [92]).

Cl_2^-, $CClF_2^-$, $C_2ClF_4^-$, and ClF^-, while in the desorption spectra we observe Cl^-, F^- and Cl_2^-.

After performing repetitive scans a new feature emerges peaking at 6 eV. Fig. 29 shows Cl^- desorption after 60 repetitive scans of 30 s each at a beam intensity of 100 nA. This new desorption feature peaking at 6 eV can be ascribed to Cl^- desorption from molecular Cl_2. This is established [92] by (i) comparing the difference spectrum (irradiated spectrum–nonirradiated spectrum) with that of a pure Cl_2 multilayer, and (ii) recording ESD spectra of irradiated samples at different temperatures. This last procedure is performed by condensing the $C_2F_4Cl_2$ film at 40 K and irradiating it at the same temperature. ESD spectra are then recorded at different temperatures. The result is that the feature due Cl_2 at 6 eV completely vanishes for temperatures above 60 K due to desorption of the Cl_2 layer. This can directly be correlated to the vapor pressure of Cl_2 in that temperature range.

Fig. 29 also shows the evolution of the F^- desorption yield in the course of 60 repetitive scans. This desorption signal is much less affected by irradiation but it should contain information on the F^- containing byproducts of the overall reaction (see the description later).

3.3.3.1. Energy dependence of Cl_2 synthesis. The most important point concerns the energy dependence of the reaction generating Cl_2. We have performed irradiation experiments at different electron energies at a 6 ML film and an irradiation time of 120 s at a beam intensity of 100 nA (corresponding to a dosage of $\approx 10^{14}$ electrons deposited). After irradiation a Cl desorption spectrum (30 s, ≈100 nA) is recorded to probe the result of irradiation. This procedure is performed stepwise for different electron energies, in each case with a newly deposited film. The result is a pronounced energy dependence for the signal intensity of the new feature at 6 eV. The peak area of this new feature is consequently assigned as *relative reaction cross section* for Cl_2 formation (Fig. 30). At this point it has to be noted that Fig. 29 reflects the conditions after exposing the film to a small electron dosage. Experiments at larger dosages indicate that for energies around 10 eV the system approaches some equilibrium while at low energies the desorption signal is completely transformed from $C_2F_4Cl_2$ to Cl_2 [94]. Fig. 30 (bottom) shows the energy-dependent charging of the film as mirrored by the shift ΔV of the electron injection curve. Charging of the film due to negative ions (parents and fragments remaining in the film) is obviously more effective at low energies than around 10 eV.

3.3.3.2. Mechanism of Cl_2 synthesis. Fig. 30 indicates that the energy dependence of the Cl_2 production cross section qualitatively follows the energy dependence of both desorption of Cl^- and charge accumulation. From the molecular point of view, electrons at 9 eV create a variety of electron-

ically excited states including electronically excited resonances which may decompose into fragments. Cl_2 can then be formed via secondary reaction sequences which are not easy to reveal. Apart from the synthesis of Cl_2, electrons of 9.5 eV energy impinging the surface will degrade both, the initial molecule, the product and also the yet not identified byproducts.

Electrons of 1 eV energy, on the other hand, can only induce a bond cleavage via the DEA process:

$$e^- + C_2F_4Cl_2 \rightarrow C_2F_4Cl + Cl^- \quad (24)$$

which is slightly exothermic by 0.2 eV. Possible secondary pathways for Cl_2 synthesis may include polymerization of the radicals formed in the first step and also reactive scattering of Cl^- as discussed in Ref. [92]. From the thermodynamic point of view we have to consider the reaction:

$$C_2F_4Cl_2 \rightarrow C_2F_4 + Cl_2 \quad (25)$$

which is the most direct way for Cl_2 synthesis. For C_2F_4 representing perfluoroethene, the reaction is endothermic by 3.0 eV [39] and thermodynamics hence predict that the chemical equilibrium is completely on the left hand side ($C_2F_4Cl_2$). As demonstrated [94], the presence of low energy electrons shift the chemical equilibrium in the condensed phase virtually to the right hand side, more precisely, to Cl_2 plus byproducts carrying the negative charge. Since any form of C_2F_4 may not posses a sufficiently high electron affinity to drive such a reaction we can assume that larger byproducts are formed. Possible scenarios are (formulated at a dimer unit).

$$e^- + 2C_2F_4Cl_2 \rightarrow (c\text{-}C_4F_8)^- + 2Cl_2 \quad (26a)$$

and

$$2e^- + 2C_2F_4Cl_2 \rightarrow 2Cl^- + c\text{-}C_4F_8 + Cl_2 \quad (26b)$$

Reaction (26a) is endothermic by 3.9 eV and would require a correspondingly high electron affinity in the perfluoro compound while (26a) is exothermic by 0.7 eV [39,92]. Thermodynamically the large electron affinity of Cl (3.6 eV) represents the driving force of reaction (26b) which we hence consider as the basic reaction relevant at subexcitation energies, and initiated via DEA. To remove the negative charges sitting on Cl^- (and eventually on undissociated c-C_4F_8) one could use low energy photons to inject the electrons into the conduction band of the metallic substrate.

One essential point necessary to achieve complete transformation is based on the fact that the initial molecule ($C_2F_4Cl_2$) is strongly affected by low energy electrons while this is not the case for the product (Cl_2). As previously shown by high resolution laser photoelectron attachment spectroscopy [95] the cross section for DEA to gas phase Cl_2 shows *p-wave* behavior resulting in a narrow peak at 50 meV at a peak cross section of $2.5 \times 10^{-20}\,m^2$. This is by about one order of magnitude lower than the DEA cross section in $C_2F_4Cl_2$. More important, this large cross section in $C_2F_4Cl_2$ extends over a much broader energy range. Finally, the perfluorinated byproducts in (26b) may not at all be affected since DEA processes are energetically inaccessible at 1 eV.

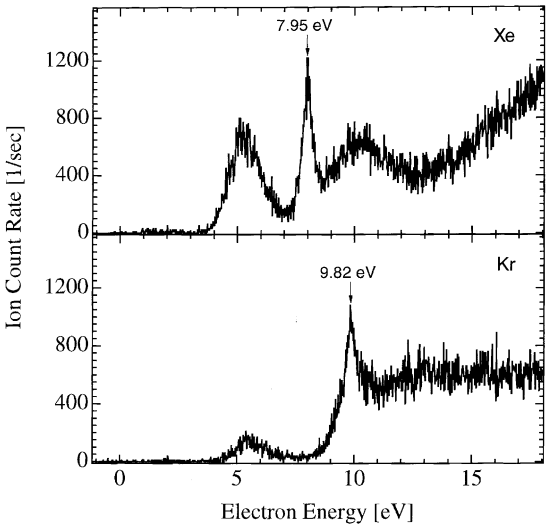

Fig. 31. Desorption yield of F^- from 0.05 ML SF_6 adsorbed on a 22 ML Kr and Xe substrate, respectively (from Ref. [96]).

Based on these facts we can further assume that the entire film of several monolayers will be transformed within the irradiated area: while the depth to monitor the Cl_2 concentration via Cl^- desorption is only in the order of one monolayer one can assume that transformation proceeds from the surface layer to the following layers.

Since the product Cl_2 (and the perfluorinated byproducts) only weakly interact with subexcitation electrons (see above) they can penetrate deeper into the film thereby transforming layer by layer. Near the surface of the metallic substrate, finally, the image charge may affect the reactions discussed above to some degree.

3.3.4. Substrate mediated reactions

In this last case study we use noble gas layers as a spacer to the metallic surface. Such a spacer can be used for two purposes: (i) to study the condensed phase effect on a molecule but to minimize the influence of the metal, and (ii) to study effects mediated by the noble gas substrate.

Fig. 31 shows desorption of F^- from SF_6 adsorbed in submonolayers (0.05 ML) on a Kr and Xe substrate, respectively [96]. In addition to the desorption features observed from a multilayer SF_6 (which have some relation to the gas phase DEA resonances [23]), from the noble gas substrate sharp enhancements at 7.95 eV (Xe) and 9.82 eV (Kr) are seen. These features are interpreted to arise from "electron/exciton complexes", i.e., an extra electron bound to an exciton in the noble gas solid. The electron/exciton complex transfers its electron *and* energy to a dissociative state of $SF_6{}^{*-}$ which decomposes into F^-. The corresponding negative ion states are well known for isolated rare gas atoms

(e.g., Kr^- ($4p^5 5s^2$) at 9.52 eV). They are observed ≈0.5 eV below the lowest excited state of the neutral atom. Similar observations have been made for D^-/D_2O and D^-/C_2D_6 [97,98]. Since SF_6 does not undergo DEA to form F^- at low energy, inelastic scattering by the noble gas substrate and dissociative capture by the slow electron can be ruled out as a possible mechanism for the sharp enhancements in the DEA cross section.

Acknowledgements

This work has been supported by the following institutions: Deutsche Forschungsgemeinschaft (DFG), Alexander von Humboldt-Stiftung, Volkswagen-Stiftung, European Union, Deutscher Akademischer Austauschdienst (DAAD), Freie Universität Berlin, NATO Research Council and Fonds der Chemischen Industrie (FCI). We are grateful to many colleagues and co-workers for valuable contributions and discussions. Their names appear in the original publications cited here. We particularly appreciate fruitful collaboration with colleagues from Orsay (Roger Azria, Michel Tronc, Yvonick Le Coat, Robert Abouaf), Innsbruck (Tilmann D. Märk, Aleksandar Stamatovic, Paul Scheier), Bratislava (Stefan Matejcik, Jan D. Skalny), Berlin (Werner F. Schmidt), Sherbrooke, Québec (Léon Sanche, Michael Huels), Washington/Athens (Loucas G. Christophorou), London/Milton Keynes (Nigel J. Mason), Bombay (E. Krishnakumar, S.V.K. Kumar), Villetaneuse (Jean-Pierre Schermannn) and Moscow (Alexei G. Khrapak, Dmitry I. Zhukhovitskii, Boris M. Smirnov). M.S. is DAAD fellow and H.A.C. is fellow of the EU Network Electron and Positron Induced Chemistry (EPIC).

References

[1] L.G. Christophorou (Ed.), Electron–Molecule Interactions and Their Applications, vol. I, Academic Press, Orlando, FL, 1984.
[2] E. Illenberger, J. Momigny, Gaseous Molecular Ions. An Introduction to Elementary Processes Induced by Ionization, Steinkopff Verlag, Darmstadt/Springer-Verlag, New York, 1992.
[3] H.S.W. Massey, E.H.S. Burhop, H.B. Gilbody, Electronic and Ionic Impact Phenomena, vol. II: Electron Collisions with Molecules and Photoionization, Clarendon Press, Oxford, 1969.
[4] H. Deutsch, K. Becker, S. Matt, T.D. Märk, Int. J. Mass Spectrom. 197 (2000) 37.
[5] D. Klar, M.-W. Ruf, H. Hotop, Int. J. Mass Spectrom. 205 (2001) 93.
[6] K.H. Becker, Elementary collision processes in plasmas, in: R. Hippler, S. Pfau, M. Schmidt, K.H. Schoenbach (Eds.), Low Temperature Plasma Physics, Wiley-VCH, Berlin, 2001.
[7] A. Grill, Cold Plasma in Material Fabrication. From Fundamental to Applications, IEE Press, New York, 1994.
[8] M. Kimura, N. Inokuti, M.A. Dillon, in: I. Prigogine, S.A. Rice (Eds.), Advances in Chemical Physics, vol. LXXXIV, Wiley, 1993.
[9] A.F. Fuciarelli, J.D. Zimbrick (Eds.), Radiation Damage in DNA: Structure/Function Relationship in Early Times, Battelle Press, Columbus-Richland, USA, 1995.
[10] B. Boudaïffa, P. Cloutier, D. Hunting, M.A. Huels, L. Sanche, Science 287 (2000) 1658.
[11] St. J. Dixon-Warren, E.T. Jensen, J.C. Polanyi, Phys. Rev. Lett. 67 (1991) 2395.
[12] J.L. Pascual, N. Lorente, Z. Song, H. Conrad, H.P. Rust, Nature 423 (2003) 535.
[13] S.W. Hla, K.-H. Rieder, Annu. Rev. Phys. Chem. 54 (2003) 307.
[14] E.P. Wigner, Phys. Rev. 73 (1948) 1002.
[15] E. Vogt, G.H. Wannier, Phys. Rev. 95 (1954) 1190.
[16] J.H. Bowie, Acc. Chem. Res. 13 (1980) 76.
[17] O. Ingólfsson, F. Weik, E. Illenberger, Int. J. Mass Spectrom. Ion Proc. 155 (1996) 1.
[18] E. Illenberger, Electron attachment reactions to free and bound molecules, in: C.Y. Ng (Ed.), Photoionization and Photodetachment, Part I and II, World Scientific, Singapore, 2000.
[19] A. Stamatovic, G.J. Schulz, Rev. Sci. Instr. 41 (1970) 423.
[20] E. Illenberger, Chem. Phys. Lett. 80 (1981) 153.
[21] W.C. Wiley, I.H. McLaren, Rev. Sci. Instr. 26 (1955) 1150.
[22] M. Meinke, E. Illenberger, J. Phys. Chem. 98 (1994) 6601.
[23] T. Oster, O. Ingólfsson, Th. Jaffke, M. Meinke, E. Illenberger, J. Chem. Phys 99 (1993) 5141.
[24] J. Langer, S. Matejcik, E. Illenberger, Int. J. Mass Spectrom. 220 (2002) 211.
[25] J. Langer, S. Matejcik, E. Illenberger, Phys. Chem. Chem. Phys. 4 (2002) 5105.
[26] A. Assion, T. Baumert, M. Bergt, T. Brixner, B. Kiefer, V. Seyfried, M. Strehle, G. Gerber, Science 282 (1998) 282.
[27] T. Brixner, H.H. Damrauer, P. Niklaus, G. Gerber, Nature 414 (2001) 57.
[28] K.A. Holbrook, M.J. Pilling, S.A. Robertson, Unimolecular Reactions, 2nd ed., Wiley, Chichester, 1996.
[29] J.L. Franklin, Energy Distribution in the Unimolecular Decomposition of Ions, vol. 1 (in Ref. [3]).
[30] M.T. Bowers (Ed.), Gas Phase Ion Chemistry, Academic Press, New York, vols. 1 and 2 (1979), vol. 3 (1984).
[31] J.H.D. Eland, Photoelectron Spectroscopy, 2nd ed., Butterworths, London, 1984.
[32] J. Berkowitz, Photoabsorption, Photoionization, and Photoelectron Spectroscopy, Academic Press, New York, 1979.
[33] C.Y. Ng (Ed.), Vacuum Ultraviolet Photoionization and Photodissociation of Molecules and Clusters, World Scientific, Singapore, 1991.
[34] C.Y. Ng (Ed.), Photoionization and Photodetachment, Part I and II, World Scientific, Singapore, 2000.
[35] R. Schinke, Photodissociation Dynamics, Cambridge Monographs on Atomic, Molecular and Chemical Physics, Cambridge University Press, 1993.
[36] J.H.D. Eland, Ion fragmentation mechanisms and photoelectron spectroscopy, in: C.R. Brundle, A.D. Baker (Eds.), Electron Spectroscopy: Theory, Techniques and Applications, vol. 4, Academic Press, London, 1979.
[37] T. Baer, J. Booze, K.-M. Weitzel, Photoelectron-Photoion Coincidence Studies of Ion Dissociation Dynamics (in Ref. [33]).
[38] K.-M. Weitzel, Unimolecular Reactions in Molecular Ions and Cluster Ions from Thermal Towards State-Selective Experiments (in Ref. [34]).
[39] http://webbook.nist.gov/chemistry.
[40] S.J. Riley, K.R. Wilson, Faraday Discuss. Chem. Soc. 53 (1972) 132.
[41] D. Krajnovich, L.J. Butler, Y.T. Lee, J. Chem. Phys. 81 (1984) 3031.
[42] H.J. Hwang, M.A. El-Sayed, J. Phys. Chem. 96 (1992) 8728.
[43] M. Burton, J.I. Magee (Eds.), Advances in Radiation Chemistry, Wiley, New York, 1969.
[44] A. Hummel, Radiation Chemistry. The Chemical Effects of Ionizing Radiation and their Applications, IRI, Technical University Delft, 1995.
[45] H. Krüger, Strahlenphysik, Dosimetrie und Strahlenschutz, Teubner, Stuttgart, 2002.

[46] A. Mozumder, Y. Hatano (Eds.), Charged Particle and Photon Interactions with Matter. Chemical, Physicochemical and Biological Consequences with Applications, Marcel Dekker, New York, 2004.
[47] S. Denifl, S. Matejcik, B. Gstir, G. Hanel, M. Probst, P. Scheier, T.D. Märk, J. Chem. Phys. 118 (2003) 74.
[48] K. Aflatooni, B. Hitt, G.A. Gallup, P.D. Burrow, J. Chem. Phys. 115 (2001) 6489.
[49] R. Abouaf, J. Pommier, H. Dunet, Int. J. Mass Spectrom. 226 (2003) 397.
[50] H. Abdoul-Carime, M.A. Huels, E. Illenberger, L. Sanche, Int. J. Mass Spectrom. 228 (2003) 703.
[51] S. Gohlke, A. Rosa, F. Brüning, M.A. Huels, E. Illenberger, J. Chem. Phys. 116 (2002) 10164.
[52] G. Hanel, B. Gstir, S. Denifl, P. Scheier, M. Probst, B. Farizon, M. Farizon, E. Illenberger, T.D. Märk, Phys. Rev. Lett. 90 (2003) 188104.
[53] H. Abdoul-Carime, M.A. Huels, L. Sanche, E. Illenberger, J. Chem. Phys. 113 (2000) 2517.
[54] H. Abdoul-Carime, L. Sanche, Radiat. Res. 153 (2000) 23.
[55] H. Abdoul-Carime, L. Sanche, Int. J. Radiat. Biol. 78 (2002) 89.
[56] E. Illenberger, Chem. Rev. 92 (1992) 1589.
[57] M. Knapp, O. Echt, D. Kreisle, E. Recknagel, J. Chem. Phys. 85 (1986) 636.
[58] H. Haberland, H. Langosch, H.-G. Schindler, D.R. Worsnop, J. Phys. Chem. 88 (1984) 3903.
[59] H. Haberland, C. Ludewigt, H.-G. Schindler, D.R. Worsnop, Surf. Sci. 156 (1985) 157.
[60] H. Haberland, C. Ludewigt, H.-G. Schindler, D.R. Worsnop, Phys. Rev. A 36 (1987) 967.
[61] H. Haberland, H.-G. Schindler, D.R. Worsnop, Ber. Bunsenges. Phys. Chem. 88 (1984) 270.
[62] L. Lehmann, E. Illenberger, Int. J. Mass Spectrom. Ion Proc. 185–187 (1999) 463.
[63] S.S. Shaik, A.B. Schlegel, S. Wolfe, Theoretical Aspects of Physical Organic Chemistry: The S_N2 Mechanism, Wiley Interscience, New York, 1992.
[64] W.N. Olmstead, J.I. Brauman, J. Am. Chem. Soc. 99 (1977) 4219.
[65] J.M. Riveros, S.M. José, K. Takashima, in: V. Gold, D. Bethell (Eds.), Advances in Physical Organic Chemistry, Academic Press, London, 1985.
[66] M.J. Pellerite, J.I. Brauman, J. Am. Chem. Soc. 105 (1983) 2672.
[67] S.L. Craig, J.I. Brauman, J. Am. Chem. Soc. 118 (1996) 6786.
[68] G. Caldwell, T.F. Maguera, P. Kebarle, J. Am. Chem. Soc. 106 (1984) 959.
[69] D.K. Bohme, G.I. Mackay, S.D. Tanner, J. Am. Chem. Soc. 102 (1980) 407.
[70] C.H. De Puy, S. Gronert, A. Mullin, V.M. Bierbaum, J. Am. Chem. Soc. 112 (1990) 8650.
[71] A.A. Viggiano, R.A. Morris, J.S. Paschkewitz, J.F. Paulson, J. Am. Chem. Soc. 114 (1992) 10477.
[72] V.F. DeTuri, P.A. Hintz, K.M. Ervin, J. Phys. Chem. A 101 (1997) 5969.
[73] D.M. Pearl, P.D. Burrow, J. Chem. Phys. 101 (1994) 2940.
[74] D.M. Pearl, P.D. Burrow, I. Fabrikant, G.A. Gullup, J. Chem. Phys. 102 (1995) 2737.
[75] N. Ruckhaberle, S. Matejcik, E. Illenberger, Y. Bouteiller, V. Périquet, L. Museur, Ch. Desfrançois, J.-P. Schermann, J. Phys. Chem. A 101 (1997) 9942.
[76] T. Oster, A. Kühn, E. Illenberger, Int. J. Mass Spectrom. Ion Process. 89 (1989) 1.
[77] J. Langer, S. Matejcik, E. Illenberger, Phys. Chem. Chem. Phys. (PCCP) 2 (2000) 1001.
[78] S. Matejcik, A. Kiendler, A. Stamatovic, T.D. Märk, Int. J. Mass Spectrom. Ion Process. 149/150 (1995) 311.
[79] P. Tegeder, E. Illenberger, Phys. Chem. Chem. Phys. 1 (1999) 5197.
[80] T. Su, R.A. Morris, A.A. Viggiano, J.F. Paulson, J. Phys. Chem. 94 (1990) 8426.
[81] L. Sanche, Phys. Rev. Lett. 53 (1984) 1638.
[82] L. Sanche, J. Phys. B: At. Mol. Opt. Phys. 23 (1990) 1597.
[83] W.T. Sturges, T.J. Wallington, M.D. Hurley, K.P. Shine, K. Sihra, A. Engel, E. Oram, S.A. Penkett, R. Mulvaney, C.A.M. Brenninkmeijer, Science 289 (2000) 611.
[84] W. Sailer, H. Drexel, A. Pelc, V. Grill, N.J. Mason, E. Illenberger, J.D. Skalny, T. Mikoviny, P. Scheier, T.D. Märk, J. Chem. Phys. 351 (2002) 71.
[85] C.L. Chen, R.E. Wotton, P.J. Chantry, in: Proceedings of the Seventh Conference of Gas Discharges and their Applications, 1982, p. 321.
[86] R. Balog, M. Stano, P. Limão-Vieira, C. König, I. Bald, N.J. Mason, E. Illenberger, J. Chem. Phys. 119 (2003) 10396.
[87] P. Tegeder, L. Lehmann, O. Ingólfsson, E. Illenberger, Zeitschr. Phys. Chem. 195 (1996) 217.
[88] A.D. Bass, J. Gamache, L. Parenteau, L. Sanche, J. Phys. Chem. 99 (1995) 6123.
[89] L. Sanche, A.D. Bass, I.I. Fabrikant, Phys. Rev. Lett. 75 (1995) 3568.
[90] Y. Le Coat, N.M. Hedhili, R. Azria, M. Tronc, O. Ingólfsson, E. Illenberger, Chem. Phys. Lett. 296 (1998) 208.
[91] F. Brüning, P. Tegeder, J. Langer, E. Illenberger, Int. J. Mass Spectrom. 195/196 (2000) 507.
[92] R. Balog, M.N. Hedhili, F. Bournel, M. Penno, M. Tronc, R. Azria, E. Illenberger, Phys. Chem. Chem. Phys. (PCCP) 4 (2002) 3350.
[93] J. Langer, M. Stano, S. Matejcik, S. Gohlke, A. Rosa, W. Barszczewska, E. Illenberger, Int. J. Mass Spectrom. 223/224 (2003) 193.
[94] R. Balog, E. Illenberger, Phys. Rev. Lett. 91 (2003) 213201.
[95] S. Barsotti, M.-W. Ruf, H. Hotop, Phys. Rev. Lett. 89 (2002) 083201-1.
[96] F. Weik, E. Illenberger, J. Chem. Phys. 109 (1998) 6079.
[97] P. Rowntree, L. Parenteau, L. Sanche, Chem. Phys. Lett. 182 (1991) 479.
[98] P. Rowntree, H. Sambe, L. Parenteau, L. Sanche, Phys. Rev. B 47 (1993) 4537.